

This discussion paper is/has been under review for the journal Atmospheric Chemistry and Physics (ACP). Please refer to the corresponding final paper in ACP if available.

# Sensitivity of simulated climate to latitudinal distribution of solar insolation reduction in **SRM** geoengineering methods

A. Modak and G. Bala

Divecha Centre for Climate Change & Centre for Atmospheric and Oceanic Sciences, Indian Institute of Science, Bangalore – 560 012, India


Received: 15 July 2013 – Accepted: 14 September 2013 – Published: 1 October 2013

Correspondence to: A. Modak (amatcaos@caos.iisc.ernet.in)

Published by Copernicus Publications on behalf of the European Geosciences Union.

25387

## Abstract

Solar radiation management (SRM) geoengineering has been proposed as a potential option to counteract climate change. We perform a set of idealized geoengineering simulations to understand the global hydrological implications of varying the latitudinal  
5 distribution of solar insolation reduction in SRM methods. We find that for a fixed total mass of sulfate aerosols (12.6 Mt of  $\text{SO}_4$ ), relative to a uniform distribution which mitigates changes in global mean temperature, global mean radiative forcing is larger when aerosol concentration is maximum at the poles leading to a warmer global mean  
climate and consequently an intensified hydrological cycle. Opposite changes are simulated  
10 when aerosol concentration is maximized in the tropics. We obtain a range of 1 K in global mean temperature and 3 % in precipitation changes by varying the distribution pattern: this range is about 50 % of the climate change from a doubling of  $\text{CO}_2$ . Hence, our study demonstrates that a range of global mean climate states, determined  
by the global mean radiative forcing, are possible for a fixed total amount of aerosols  
15 but with differing latitudinal distribution, highlighting the need for a careful evaluation of SRM proposals. 

## 1 Introduction

Atmospheric concentrations of the greenhouse gases (GHGs) such as carbon dioxide ( $\text{CO}_2$ ), methane ( $\text{CH}_4$ ) and nitrous oxide ( $\text{N}_2\text{O}$ ) have been increasing since pre-  
20 industrial periods primarily because of fossil fuel use and land-use change (IPCC, 2007). Their increase has the potential to cause long term climate change by altering the planetary radiation budget. To moderate future climate change and its impacts, several geoengineering proposals have been made recently. By definition, geoengineering is an intentional large-scale manipulation of the environment, particularly intended to counteract the undesired consequences of anthropogenic climate change  
25 (Keith, 2000).

25388

Discussion Paper | Discussion Paper | Discussion Paper | Discussion Paper | Discussion Paper

Discussion Paper | Discussion Paper | Discussion Paper | Discussion Paper

Proposed geoengineering methods are classified into two main groups: Solar Radiation Management (SRM) methods and Carbon dioxide Removal (CDR) methods (Shepherd et al., 2009). In the first approach, the amount of solar absorption by the planet is reduced by artificially enhancing the planetary albedo so that the reduced insolation compensates the radiative forcing due to rising GHGs. Some proposed methods are injecting sulfate aerosols in the stratosphere (Budkyo, 1982; Crutzen, 2006; Wigley, 2006) and placing space based sun shields in between the Sun and the Earth (Early, 1989). CDR methods propose to accelerate the removal of CO<sub>2</sub> from the atmosphere and thus they deal with the root cause of global warming (The Royal Society, 2009).

Past climate modeling studies have modeled the effects of space-based SRM methods by reducing the solar constant (Govindasamy and Caldeira, 2000; Matthews and Caldeira, 2007; Caldeira and Wood, 2008; Lunt et al., 2008) or modeled the effects of stratospheric aerosol methods (Robock et al., 2008; Rasch et al., 2008a, b; Heckendorn et al., 2009; Jones et al., 2010). It has been shown (Bala et al., 2008) that SRM geoengineering would lead to a weakening of the global water cycle when the global mean temperature change is mitigated exactly. Further, it has been shown (Robock et al., 2008; Ricke et al., 2010) that the level of compensation will vary with residual changes larger in some regions than others. Therefore, some recent studies (Ban-Weiss and Caldeira, 2010; MacMartin et al., 2012) determine an optimal reduction in solar radiation in both space and time so the geoengineered world is more similar to the control climate while other studies (Irvine et al., 2010; Ricke et al., 2010) analyze the effect of different levels of uniform SRM forcing on regional climate response. Ban-Weiss and Caldeira (2010) vary both the amount and latitudinal distribution of aerosols to mitigate either the zonally averaged changes in surface temperature or the water budget. However, a simple and clear understanding of the effects of varying the latitudinal distribution of aerosols and hence solar insolation reduction (e.g. more concentration in the tropics or high latitudes) on the hydrological cycle and surface temperature is lacking. In this study, we perform multiple idealized SRM geoengineering simulations

25389

with constant total amount of sulfate aerosols but with systematically varying latitudinal distribution.

We caution that our simulations are highly idealized and they are not meant to represent realistic latitudinal distribution of aerosols in geoengineering scenarios. Rather, they are designed to elucidate the fundamental properties of the climate system when the latitudinal distribution of aerosols and hence solar insolation reduction is systematically altered. We believe that our study should be considered as complementary to a previous work (Ban-Weiss and Caldeira, 2010), because not only we vary the latitudinal distribution of aerosols but we also provide a constraint by fixing the total amount of aerosols which facilitates a clear insight on the effects of varying the latitudinal distribution of aerosols.

## 2 Model and experiments

We used the atmospheric general circulation model, CAM3.1 developed at the National Center for Atmospheric Research (NCAR) (Collins et al., 2004). It is coupled to the land model CLM3.0 and to a slab ocean model (SOM) with a thermodynamic sea ice model to represent the interactions with the ocean and sea ice components of the climate system. The model can be also configured with prescribed sea surface temperature and sea ice fraction. The horizontal resolution is 2° latitude and 2.5° longitude and the model has 26 vertical levels and the top of the model (TOM) is at 3 hPa.

We performed two sets of simulations: (1) fixed-SST (sea surface temperature) simulations to estimate the radiative forcing which is measured as the net radiative flux change at the top of the atmosphere (Hansen et al., 1997). (2) The other set include the SOM simulations to study the climate change. For both set of simulations, fixed-SST and SOM, we performed twelve cases: a control (1 × CO<sub>2</sub>), doubled CO<sub>2</sub> climate (2 × CO<sub>2</sub>) and ten geoengineering simulations each with differing latitudinal distribution of sulfate aerosol concentrations but with fixed total amount. The concentration of atmospheric CO<sub>2</sub> in 1 × CO<sub>2</sub> is 390 ppm and is 780 ppm in 2 × CO<sub>2</sub> and geoengineering

25390

simulations. The concentrations of other greenhouse gases are kept constant in all simulations. The background sulfate aerosol amount in this version of the model is 1.38 Mt  $\text{SO}_4$ . The fixed-SST simulations lasted for 30 yr and the last 20 yr are used to calculate the radiative forcing. The SOM simulations lasted for 60 yr and the last 30 yr are used for climate change analysis since all SOM simulations reach a near-equilibrium climate state in approximately 25 yr.

In each of the geoengineering simulations (Table 1, Fig. 1a) aerosol mass is added to the model background concentration at the TOM as was done in a recent study (Ban-Weiss and Caldeira, 2010). As in Ban-Weiss and Caldeira (2010), this additional sulfate is prescribed and hence it is not transported around. However, in contrast to Ban-Weiss and Caldeira (2010), we introduce the constraint that the total amount of aerosol is constant (12.6 Mt  $\text{SO}_4$ ) while latitudinal distributions are varied. Since aerosols are prescribed at TOM, the effect is essentially equivalent to making latitudinal changes to the solar constant. Sulfate aerosol particle size is prescribed and is assumed to be log-normally distributed with dry median radius  $\approx 0.05 \mu\text{m}$  and geometric standard deviation  $\approx 2.0$  (as used in a geoengineering scenario in a previous study, Rasch et al., 2008b). The aerosol indirect effects are not modeled and aerosol loadings for other species like sea-salt, soil dust, black and organic carbon are unchanged in each of the simulations.

Besides a simulation with uniform aerosol concentration, our geoengineering simulations can be grouped into two categories: (1) Three “Tropics” simulations with maximum aerosol concentrations at the equator and (2) Six “Polar” cases with maximum concentrations at the poles. The latitudinal distribution of the stratospheric sulfate aerosol concentration are developed using the expression:

$$Q(\varphi) = a + b\cos(\varphi) \quad (1)$$

where  $Q$  is the concentration of the additional mass of sulfate aerosols,  $a$  and  $b\cos(\varphi)$  are the uniform and non-uniform components of the distributions and  $\varphi$  represents the latitude. Both  $a$  and  $b$  are varied to obtain various distributions of concentrations

25391

(Table 1, Fig. 1a). However, when  $Q$  is integrated over the sphere, the result is 12.6 Mt in all the cases. Our choice of 12.6 Mt for  $Q$  is dictated by the uniform distribution case which had near-zero global mean temperature change relative to the control case.

### 3 Results

#### 3.1 Global mean temperature and precipitation response

We find that the radiative forcing for doubling the atmospheric  $\text{CO}_2$  ( $2 \times \text{CO}_2$ ) to be  $3.5 \text{ W m}^{-2}$  while the global mean surface temperature rise is about 2.1 K and the precipitation increase is about 4.3 % (i.e.  $\approx 2 \% \text{ K}^{-1}$ ) in agreement with previous studies using the same model (Rasch et al., 2008b; Bala et al., 2009). The slopes in Fig. 1c and 1d indicate a climate sensitivity of  $0.53 \text{ K (Wm}^{-2}\text{)}^{-1}$  and precipitation sensitivity (% change in precipitation for unit change in radiative forcing) of  $1.53 \% (\text{Wm}^{-2}\text{)}^{-1}$  respectively, values that are similar to Bala et al. (2009).

The slight warming in the geoengineering case where forcing is close to zero (Fig. 1c) is because of the  $\text{CO}_2$  physiological forcing (Betts et al., 2007; Cao et al., 2010) which is not counteracted by a decrease in solar flux.  $\text{CO}_2$  physiological forcing refers to the direct physiological response of plants to elevated  $\text{CO}_2$ : the plant stomata open less widely and thus decrease the canopy transpiration which in turn reduces evapotranspiration and causes surface warming. Therefore, in the zero radiative forcing case where  $\text{CO}_2$  radiative forcing is countered by the reduction in solar radiation, the  $\text{CO}_2$ -physiological forcing leads to a slight warming.

In agreement with past studies (e.g. Lunt et al., 2008; Bala et al., 2008), we find that in the geoengineering scenario with uniform distribution of aerosol there is a decline in precipitation though the temperature change is completely mitigated (Fig. 1b). This occurs because of differing fast response in precipitation for solar and  $\text{CO}_2$ -forcing (Allen and Ingram, 2002; Bala et al., 2008, 2009; Andrews et al., 2009).  $\text{CO}_2$ -forcing heats the troposphere, increases the vertical stability and thus leads to precipitation suppres-

25392

sion (Cao et al., 2012). In contrast, solar forcing tends to heat the atmosphere only slightly causing much smaller change in precipitation. Therefore, in a geoengineered world the precipitation suppression caused by CO<sub>2</sub>-forcing is not mitigated by the specified amount of solar forcing which mitigates temperature change. This suppression of precipitation is simulated in all geoengineering simulations (the regression line does not pass through the origin in Fig. 1b). Therefore the precipitation change in any geoengineering simulation can be inferred from the linear relationship between changes in precipitation and temperature changes and the fast response component.

Our geoengineering simulations with varying aerosol distributions indicate a linear relationship between the global mean surface temperature change and the precipitation change (Fig. 1b). The regression lines do not pass through the origin which implies that none of the distribution can mitigate global mean temperature and precipitation simultaneously. Though the total amount of aerosols in each of the geoengineering simulation is fixed, we obtain a range of 1 K (residual cooling of 0.3 K for the Tropics3 case to residual warming of 0.7 K for the Polar6 case) in global mean temperature and 3 % (residual drying of 2 % for Tropics3 case to residual increase of 1 % for the Polar6 case) in precipitation changes which are about 50 % or more of the changes that result from doubling of CO<sub>2</sub>. This indicates that a range of climate states are possible for a constant amount of aerosols.

As the polar maximum of the aerosol concentration increases the global mean temperature increases with concomitant increase in global mean precipitation as implied by the linear relationship in Fig. 1b. One of the polar maximum SRM simulations (Polar3) almost offsets the changes in global mean precipitation but it has a residual warming of 0.4 °C. Our results are broadly in agreement with other modeling studies: in an Arctic geoengineering study (Caldeira and Wood, 2008) with reduced solar constant only over arctic, residual global mean warming and enhancements of global precipitation are found.

In contrast, as magnitude of the tropical maximum concentration increases both global mean temperature and precipitation decreases. One of the Tropics cases (Trop-

25393

ics1) where the temperature change is nearly zero shows a reduction in the global mean precipitation. The reduction in precipitation in our “Tropics” simulations are consistent with observed decline in precipitation over land, runoff and river discharge into the ocean following the tropical volcanic eruption Mount Pinatubo (15° N) in 1991 (Trenberth and Dai, 2007). **Interestingly, we find that in none of the geoengineering scenarios changes in global mean surface temperature and precipitation can be mitigated simultaneously over either land or ocean.** We also notice that the hydrological sensitivity (% change in precipitation per unit change in temperature) is almost same over both land and ocean (Fig. 1b). Here, we have defined the hydrological sensitivity over land (ocean) as the ratio of change in land (ocean) averaged precipitation to change in land (ocean) averaged surface temperature.

We find that the prescribed aerosols with different latitudinal distributions along with doubled CO<sub>2</sub> concentrations (geoengineering simulations) lead to different global mean forcings (Fig. 1c and d). Since there are linear relationships between radiative forcing and the changes in global mean temperature (Fig. 1c) and between temperature and precipitation changes (Fig. 1b), we find a linear relationship between radiative forcing and precipitation changes (Fig. 1d). The Polar geoengineering scenarios have positive residual radiative forcing while the Tropics scenarios have negative residual forcing because solar forcing is less effective over the poles relative to the tropics (Fig. 1c). This is further confirmed in Fig. 2 which shows that the Polar cases have smaller increase in planetary albedo compared to the Tropics cases. The radiative forcing associated with planetary albedo changes drive the temperature changes and thus the Polar cases have lower albedo changes relative to the uniform case and hence are warmer and wetter while opposite is true for Tropics cases.

The variation of global mean surface temperature and precipitation with global mean radiative forcing (Fig. 1c and 1d) shows that as the maximum aerosol concentration over the poles increases (Polar1 to Polar6) the residual forcing increases and hence the global mean temperature and precipitation increase. Similarly, as the maximum

25394

aerosol concentration over the equator increases (Tropics1 to Tropics3), an opposite variation is noticed.

The root mean square difference (RMSD) of the geoengineering simulations with respect to the control case, normalized by the spatial standard deviation in the control scenario shows that the RMSD in temperature increases as the maximum concentration of aerosols at the poles increases and the RMSD in precipitation increases as tropical maximum is increased (Fig. 3). We normalize RMSD by standard deviation in the control scenario so the RMSD between a geoengineered and a control world can be compared to the regional variations in the control simulation. Figure 3a shows the ratio of spatial RMSD and standard deviation of the control simulation while the ratio of zonal mean RMSD and standard deviation is shown in Fig. 3b. In case of spatial RMSD the spread is more, 0.40 to 1.4 for surface temperature and 0.25 to 0.40 for precipitation. In case of RMSD in zonal means, the spread is relatively less: 0.30 to 0.95 for surface temperature and 0.27 to 0.38 for precipitation. The uniform case has the least distance from the origin in Fig. 3, suggesting that it has the least RMSD if the objective is to minimize RMSD in both temperature and precipitation simultaneously.

### 3.2 Precipitation and temperature response in Tropics and Poles

The change in zonal-mean surface temperature between the geoengineering cases and the control case ( $1 \times \text{CO}_2$ ) show, similar to changes in global annual mean values, a monotonic increase at each latitude with increased polar weighting (Fig. 4a). We notice a similar monotonic increase in zonal-mean land and zonal-mean ocean surface temperature (Fig. 5a and 5b). Further, we find that almost all geoengineering simulation show residual high latitude warming. In the Tropics cases, we find smaller residual warming in the high latitudes and cooler tropics. Similar to temperature changes, the change in zonal-mean precipitation between the geoengineering cases and the control case show a monotonic increase at each latitude with increased polar weighting (Figs. 4b, 5c and 5d). We find large changes in precipitation in the tropics which is likely to be seen as shifts in the intertropical convergence zone (ITCZ) but closer examina-

25395

tion (Fig. 6) shows that the position of ITCZ remains the same in all the cases and the monotonic increase in precipitation with poleward weighting is clearly seen. The changes in zonal mean precipitation minus evaporation (water budget) are similar to changes in zonal mean precipitation (Figs. 4c, 5e and 5f).

Figure 7 shows the spatial pattern of radiative forcing in selected simulations:  $2 \times \text{CO}_2$ , Uniform, Polar3, Tropics1, Polar6 and Tropics3 cases. We notice that the radiative forcing in the  $2 \times \text{CO}_2$  case is significant over the whole globe but not significant in most regions in the geoengineering cases. The radiative forcing is positive in most locations in case of Polar cases. In the Tropics cases, the forcing is negative in the tropical regions and positive in polar regions.

In the  $2 \times \text{CO}_2$  case, both temperature and precipitation changes are large and significant over the whole globe (Fig. 8). The temperature increase over poles is much larger than in the tropics, in agreement with previous studies (Caldeira and Wood, 2008; Lun-tet al., 2008; Matthews and Caldeira, 2007; Roboquet al., 2008; Rasch et al., 2008b). The uniform geoengineering case (Uniform) shows mitigation in the temperature with reduced precipitation relative to  $1 \times \text{CO}_2$ . This is because of the different nature of the  $\text{CO}_2$  forcing and solar forcing: solar forcing is larger in the tropics and smaller in the poles whereas the  $\text{CO}_2$  forcing is uniform over the whole globe. In Polar3 case, the change in precipitation is largely mitigated but there is significant warming over large regions. However, temperature is largely mitigated in Tropics1 but there is decrease in precipitation relative to the uniform distribution case. The last four panels of Fig. 8 shows the extreme cases; the case with largest polar weighting (Polar6) significantly warms the planet while the case with largest tropical weighting (Tropics3) overcools the planet with large reduction in precipitation. The seasonal variations in residual temperatures mostly occur in the high latitudes with stronger response in the winter and weaker response in the summer (Fig. 9) following the seasonal cycle of radiative forcing (Fig. 7; right panels). The magnitude of seasonal variations in precipitation response is large in the tropics in the geoengineering cases but with reduced intensity compared to the  $2 \times \text{CO}_2$  case.

#### 4 Discussion and conclusions

In this study, we find that when the latitudinal distribution of sulfate aerosols is altered the global mean radiative forcing changes which leads to changes in surface temperature as indicated by the climate sensitivity of the model (Fig. 1c). Consequent changes in global mean precipitation are simulated as dictated by the hydrological sensitivity of the model (Fig. 1b). We also observe a similar monotonic increase in precipitation intensity as the maximum aerosol concentration over the poles increases (Fig. 10). The increases are of the order of 10 % for low intensity (5th percentile) and 2–3 % for large intensity (99th percentile) between the extreme cases (Tropics3 and Polar6). In order to confirm that global mean radiative forcing is sufficient to infer the global mean climate change we performed four additional geoengineering simulations with total amount of aerosols varied (10 Mt, 11 Mt, 13 Mt and 14 Mt) for the uniform distribution case. We find that the global mean temperature and precipitation changes follow the changes in global mean forcing (Fig. 11) for this set of simulations too.

In agreement with earlier studies (e.g. Bala et al., 2008), we find that both temperature and precipitation changes cannot be mitigated simultaneously in all geoengineering simulations considered in this study (that is, even with non-uniform distribution of solar insolation reduction). The latitudinal distribution which offsets the warming leads to a drier climate while the distribution which offsets the precipitation results in a relatively warmer world (note that Bala et al. (2008) used a uniform solar insolation reduction). For a fixed total amount of aerosols but with different latitudinal distribution it is possible to achieve a range of global mean radiative forcing and thus a range of climate states.

Our findings should be viewed in the light of the limitations and uncertainties involved in this study. Our simulations are highly idealized as we have prescribed sulfate aerosol (to reduce the solar insolation) instead of injecting and transporting them. We have prescribed a fixed particle size distribution but particle size distribution would evolve with time and is shown to be important in precisely estimating the effects on different climate

25397

variables (Rasch et al., 2008b). Some modeling studies (Robock et al., 2008) have injected aerosol precursors into to the stratosphere with fixed particle size distribution while other studies (Heckendorn et al., 2009; Pierce et al., 2010; Niemeier et al., 2010; Hommel and Graf, 2011; English et al., 2012) have demonstrated the importance of including the microphysics of particle growth. Further, we have focused our investigation primarily on global mean climate while several other studies (e.g. Robock et al., 2008; Irvine et al., 2010; Ricke et al., 2010) focused on regional disparities.

In this study, we have not considered the consequences of sulfate aerosol chemistry on the ozone layer (Tilmes et al., 2009). Our model lacks a dynamic ocean and sea ice components and the effects of deep ocean circulation are not modeled here. However, we believe our results on temperature and precipitation is so fundamental that they would be unchanged when additional components and feedbacks are included.

In summary, for a fixed total mass of aerosols, we find that the global mean climate is warmer and wetter when aerosol concentration is maximum over the poles relative to the uniform distribution case (which mitigates global mean temperature change) because the global mean residual radiative forcing is positive in these cases when compared to the uniform case. The opposite is true when aerosol concentration is maximum in the tropics. Further, our study clearly indicates that knowledge of global mean radiative forcing, not the details of latitudinal distribution of aerosols, is sufficient to infer the global mean climate change.

*Acknowledgements.* Financial support for A. Modak was provided by the Divecha Centre for Climate Change, Indian Institute of Science. We thank the Supercomputer Education and Research Centre, Indian Institute of Science for providing the computational resources.

#### References

Allen, M. R. and Ingram, W. J.: Constraints on future changes in climate and the hydrologic cycle, *Nature*, 419, 224–232, doi:10.1038/nature01092, 2002.

25398

- Andrews, T., Forster, P. M., and Gregory, J. M.: A surface energy perspective on climate change, *J. Climate.*, 22, 2557–2570, doi:10.1175/2008JCLI2759.1, 2009.
- Bala, G., Caldeira K., and Nemani, R.: Fast versus slow response in climate change: implications for the global hydrological cycle, *Clim. Dynam.* 35, 423–434, doi:10.1007/s00382-009-0583-y, 2009.
- 5 Bala, G., Duffy P. B., and Taylor, K. E.: Impact of geoengineering schemes on the global hydrological cycle, *P. Natl. Acad. Sci. USA*, 105, 7664–7669, doi:10.1073/pnas.0711648105, 2008.
- Ban-Weiss, G. A. and Caldeira, K.: Geoengineering as an Optimization Problem, *Environ. Res. Lett.*, 5, 034009, doi:10.1088/1748-9326/5/3/034009, 2010.
- 10 Betts, R. A., Boucher, O., Matthew, C., Cox, P. M., Falloon, P. D., Gedney, N., Hemming, D. L., Huntingford, C., Jones, C. D., Sexton, D. M. H., and Webb, M. J.: Projected increase in continental runoff due to plant responses to increasing carbon dioxide, *Nature*, 448, 1037–1041, doi:10.1038/nature06045, 2007.
- 15 Budkyo, M. I.: *The Earth's Climate Past and Future*, Academic, 1982.
- Caldeira, K. and Wood, L.: Global and Arctic climate engineering: Numerical model studies, *Philos. T. Roy. Soc. A*, 366, 4039–4056, doi:10.1098/rsta.2008.0132, 2008.
- Cao, L., Bala, G., Caldeira, K., Nemani, R., and Ban-Weiss, G. A.: Importance of carbon dioxide physiological forcing to future climate change, *P. Natl. Acad. Sci. USA*, 107, 9513–9518, doi:10.1073/pnas.0913000107, 2010.
- 20 Cao, L., Bala, G., and Caldeira, K.: Climate response to changes in atmospheric carbon dioxide and solar irradiance on the time scale of days to weeks, *Environ. Res. Lett.*, 7, 034015, doi:10.1088/1748-9326/7/3/034015, 2012.
- Collins, W. D., Rasch, P. J., Boville, B. A., Hack, J. J., McCaa, J. R., Williamson, D. L., Kiehl, J. T., Briegleb, B., Bitz, C., Lin, S.-J., Zhang, M., and Dai, Y.: Description of the NCAR community atmosphere model (CAM 3.0) NCAR Tech. Rep. NCAR/TN-464+STR National Center for Atmospheric Research Boulder CO 226 pp., 2004.
- 25 Crutzen, P. J.: Albedo enhancement by stratospheric sulfur injections: A contribution to resolve a policy dilemma?, *Climatic Change*, 77, 211–220, doi:10.1007/s10584-006-9101-y, 2006.
- 30 Early, J. T.: Space-based solar shield to offset greenhouse effect, *JBIS-J. Brit. Interpla.*, 42, 567–569, 1989.

25399

- English, J. M., Toon, O. B., and Mills, M. J.: Microphysical simulations of sulfur burdens from stratospheric sulfur geoengineering, *Atmos. Chem. Phys.*, 12, 4775–4793, doi:10.5194/acp-12-4775-2012, 2012.
- Govindasamy, B. and Caldeira, K.: Geoengineering Earth's radiation balance to mitigate CO<sub>2</sub>-induced climate change, *Geophys. Res. Lett.*, 27, 2141–2144, 2000.
- 5 Hansen, J., Sato, M., and Ruedy, R.: Radiative forcing and climate response, *J. Geophys. Res.*, 102, 6831–6864, 1997.
- Heckendorn, P., Weisenstein, D., Fueglistaler, S., Luo, B. P., Rozanov, E., Schraner, M., Thomason, L. W., and Peter, T.: The impact of geoengineering aerosols on stratospheric temperature and ozone, *Environ. Res. Lett.*, 4, 045108, doi:10.1088/1748-9326/4/4/045108, 2009.
- 10 Hommel, R. and Graf, H. F.: Modelling the size distribution of geoengineered stratospheric aerosols, *Atmos. Sci. Lett.*, 12, 168–175, doi:10.1002/asl.285, 2011.
- Irvine, P. J., Ridgwell, A., and Lunt, D. J.: Assessing the regional disparities in geoengineering impacts, *Geophys. Res. Lett.*, 37, L18702, doi:10.1029/2010GL044447, 2010.
- 15 IPCC 2007 Climate Change 2007: The Physical Science Basis Contribution of Working Group 1 to the Fourth Assessment Report of the Intergovernmental Panel on Climate Change ed Solomon, S., Qin, D., Manning, M., Chen, Z., Marquis, M., Averyt, K. B., Tignor, M., and Miller, H. L.: (Cambridge & New York: Cambridge University Press) 996 pp., 2007.
- Jones, A., Haywood, J., Boucher, O., Kravitz, B., and Robock, A.: Geoengineering by stratospheric SO<sub>2</sub> injection: results from the Met Office HadGEM2 climate model and comparison with the Goddard Institute for Space Studies ModelE, *Atmos. Chem. Phys.*, 10, 5999–6006, doi:10.5194/acp-10-5999-2010, 2010.
- 20 Keith, D. W.: Geoengineering the climate: history and prospect, *Annu. Rev. Energ. Env.*, 25, 245–284, 2000.
- 25 Lunt, D. J., Ridgwell, A., Valdes, P. J., and Seale, A.: 'Sunshade world': a fully coupled GCM evaluation of the climatic impacts of geoengineering, *Geophys. Res. Lett.*, 35, L12710, doi:10.1029/2008GL033674, 2008.
- MacMartin, D. G., Keith, D. W., Kravitz, B., and Caldeira, K.: Management of trade-offs in geoengineering through optimal choice of non-uniform radiative forcing, *Nature Climate Change*, 3, 365–368, doi:10.1038/nclimate1722, 2012.
- 30 Matthews, H. D. and Caldeira, K.: Transient climate-carbon simulations of planetary geoengineering, *P. Natl. Acad. Sci. USA*, 104, 9949–9954, doi:10.1073/pnas.0700419104, 2007.

25400

- Niemeier, U., Schmidt, H., and Timmreck, C.: The dependency of geoengineered sulfate aerosol on the emission strategy, *Atmos. Sci. Lett.*, 12, 189–194, doi:10.1002/asl.304, 2010.
- Pierce, J. R., Weisenstein, D. K., Heckendorn, P., Peter, T., and Keith, D. W.: Efficient formation of stratospheric aerosol for climate engineering by emission of condensable vapor from aircraft, *Geophys. Res. Lett.*, 37, L18805, doi:10.1029/2010GL043975, 2010.
- Rasch, P. J., Tilmes, S., Turco, R. P., Robock, A., Oman, L., Chen, C. C., Stenchikov, G. L., and Garcia, R. R.: An overview of geoengineering of climate using stratospheric sulphate aerosols, *Philos. T. Roy. Soc. A*, 366, 4007–4037, doi:10.1098/rsta.2008.0131, 2008a.
- Rasch, P. J., Crutzen, P. J., and Coleman, D. B.: Exploring the geoengineering of climate using stratospheric sulfate aerosols: The role of particle size, *Geophys. Res. Lett.*, 35, L02809, doi:10.1029/2007GL032179, 2008b.
- Ricke, K. L., Morgan, M. G., and Allen, M. R.: Regional climate response to solar-radiation management, *Nat. Geosci.*, 3, 537–541, 2010.
- Robock, A., Oman, L., and Stenchikov, G. L.: Regional climate responses to geoengineering with tropical and Arctic SO<sub>2</sub> injections, *J. Geophys. Res.*, 113, D16101, doi:10.1029/2008JD010050, 2008.
- Shepherd, J., Caldeira, K., Haigh, J., Keith, D., Launder, B., Mace, G., MacKerron, G., Pyle, J., Rayner, S., Redgwell, C., and Watson, A.: *Geoengineering the climate: science, governance and uncertainty*, The Royal Academy, 2009.
- Tilmes, S., Garcia, R. R., Kinnison, D. E., Gettelman, A., and Rasch, P. J.: Impact of geoengineered aerosols on the troposphere and stratosphere, *J. Geophys. Res.*, 114, D12305, doi:10.1029/2008JD011420, 2009.
- Trenberth, K. E. and Dai, A.: Effects of Mount Pinatubo volcanic eruption on the hydrological cycle as an analog of geoengineering, *Geophys. Res. Lett.*, 34, L15702, doi:10.1029/2007GL030524, 2007.
- Wigley, T. M. L.: A combined mitigation/geoengineering approach to climate stabilization, *Science*, 314, 452–454, doi:10.1126/science.1131728, 2006.

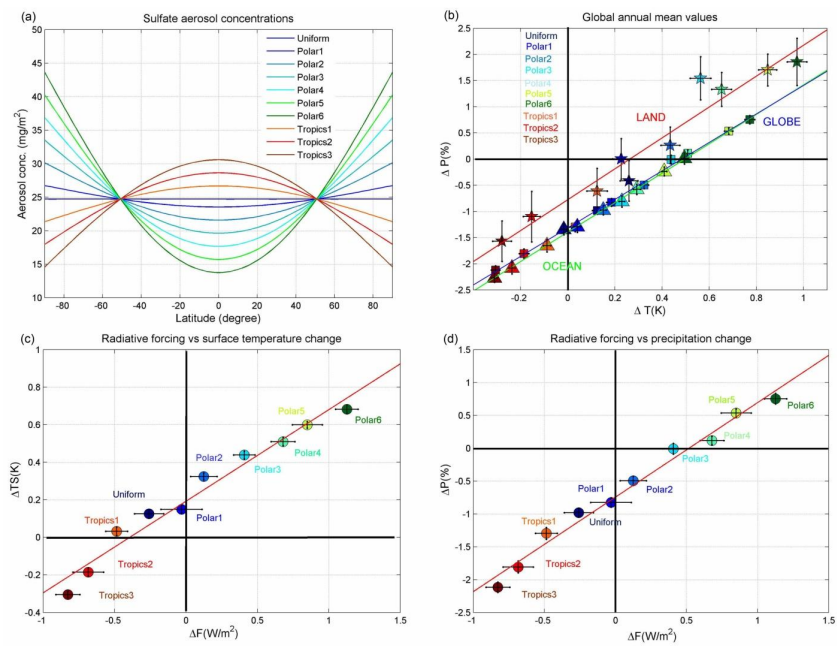
25401

**Table 1.** Description of different geoengineering experiments. Total additional mass is 12.6 Mt SO<sub>4</sub> in all the geoengineering simulations but the distribution varies.

Name of the Experiments	<i>a</i> (mg m <sup>-2</sup> )	<i>b</i> (mg m <sup>-2</sup> )	Total Mass from uniform component (Mt)	Total Mass from non-uniform component (Mt)	Total Mass (Mt)
Uniform	24.70	–	12.60	–	12.60
Polar1	23.52	3.19	12.00	0.60	12.60
Polar2	21.56	8.55	11.00	1.60	12.60
Polar3	19.60	13.89	10.00	2.60	12.60
Polar4	17.64	19.22	9.00	3.60	12.60
Polar5	15.68	24.56	8.00	4.60	12.60
Polar6	13.72	29.90	7.00	5.60	12.60
Tropics1	26.66	–5.34	13.60	–1.00	12.60
Tropics2	28.62	–10.67	14.60	–2.00	12.60
Tropics3	30.58	–16.02	15.60	–3.00	12.60

25402





25403

**Fig. 1.** (a) Latitudinal profiles of sulfate aerosol concentration in the SRM geoengineering experiments. Polar1–6 have maximum concentration over the poles and Tropics1–3 have maximum at the equator. (b) Surface temperature change (K) vs. precipitation change (%) relative to the 1xCO<sub>2</sub> case from slab ocean simulations (global mean values – squares, land mean values – stars, ocean mean values – triangles). There is warming in all Polar cases relative to the uniform case and a concomitant increase in precipitation. Opposite is the case for Tropics cases. None of the regression lines pass through origin; temperature and precipitation cannot be mitigated simultaneously. In the case of land and ocean, ΔT<sub>S</sub> and ΔP represent the averages over the respective domain. (c) Radiative forcing (RF) vs. surface temperature change. Polar cases have larger forcing relative to the uniform case and hence are warmer while opposite is true for Tropics cases. (d) Radiative forcing vs. % precipitation change. Precipitation increases with residual RF (i.e. with increase in polar weighting) while decreases with increase in tropical weighting. In (b), (c) and (d) the horizontal and vertical bars represent the standard error of the respective variables which are calculated from the last 30 yr of 60 yr SOM simulations while in case of radiative forcing it is calculated from the last 20 yr of 30 yr fixed-SST simulations.

25404

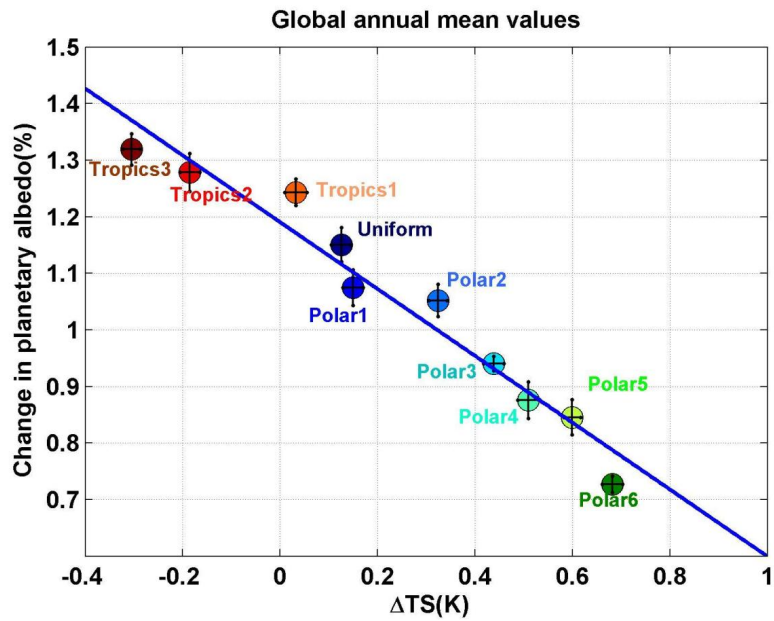
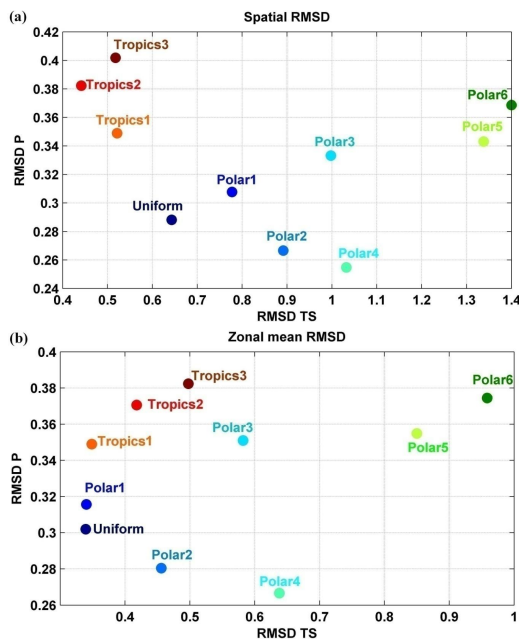


**Fig. 2.** Change in planetary albedo in fixed-SST vs. surface temperature change in slab ocean geoengineering simulations. The radiative forcing associated with albedo changes drive the temperature changes. Polar cases have lower albedo changes relative to the uniform case and hence are warmer and wetter while opposite is true for Tropics cases. The horizontal and vertical bars represent the standard error of the respective variables; temperature standard errors are calculated from the last 30 yr of 60 yr SOM simulations while albedo standard errors are calculated from the last 20 yr of 30 yr fixed-SST simulations.

25405



25406

**Fig. 3.** Root mean square difference (RMSD) of surface temperature and precipitation between geoengineering and control simulation normalized by spatial standard deviation in the control scenario computed for the global domain (top panel) and for the zonal averages (bottom panel). The annual means of the last 30 yr of the 60 yr control simulation are used to estimate the standard deviation. Simulation nearest to x axis represents the best precipitation mitigating scenario while the one closest to y axis represents the best surface temperature mitigating scenario. Scenarios with maximum aerosol concentrations at the poles have larger RMSD in temperature and conversely simulations with maximum at the equator have larger RMSD in precipitation.

25407

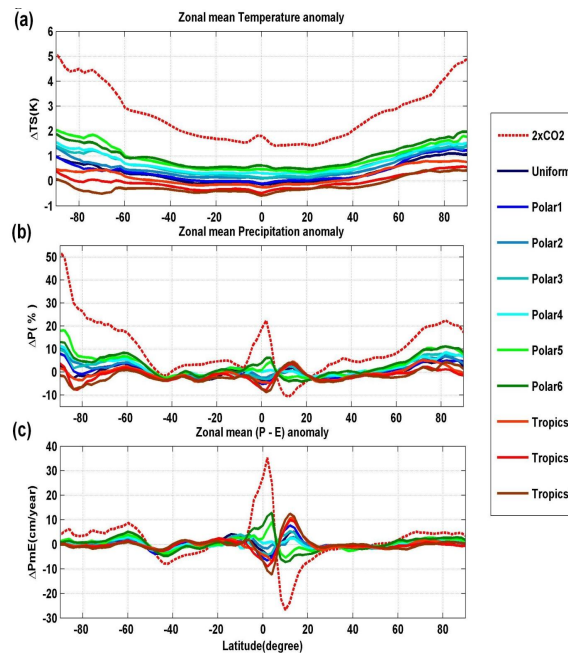


**Fig. 4.** Zonal means of change in surface temperature ( $\Delta TS$ ), precipitation ( $\Delta P$ ) and precipitation minus evaporation ( $\Delta PmE$ ). **(a)** Zonal mean  $\Delta TS$  increases monotonically with increase in maximum concentrations over the poles and decreases with increase in tropical maxima. **(b)** Zonal mean  $\Delta P$ : polar maximum causes enhanced precipitation. **(c)** Zonal mean  $\Delta PmE$ : polar maximum causes enhanced precipitation minus evaporation. Results shown are averages of the last 30 yr of 60 yr simulations.

25408

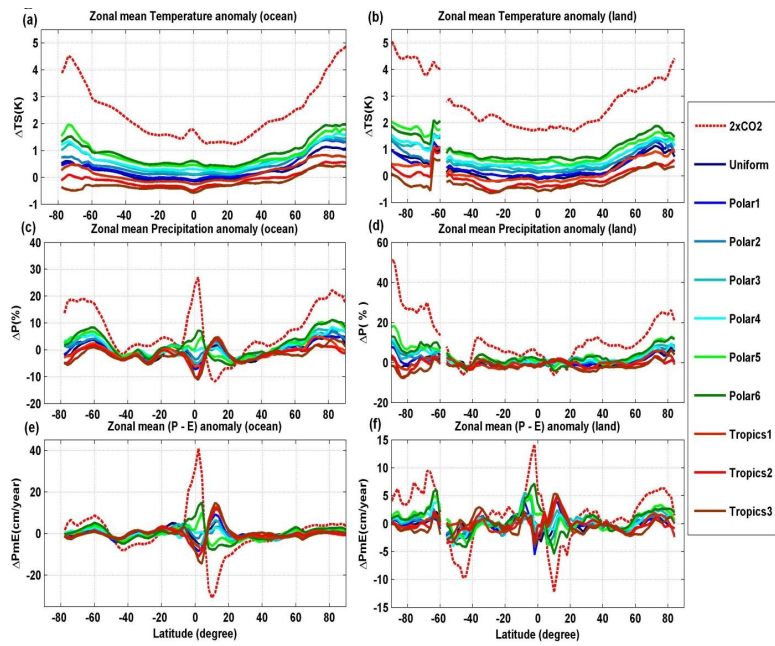


**Fig. 5.** Changes in zonal mean surface temperature ( $\Delta TS$ ), precipitation ( $\Delta P$ ) and precipitation minus evaporation ( $\Delta PmE$ ) over ocean (left panels) and land (right panels). **(a, b)** Zonal mean  $\Delta TS$  increases monotonically with increase in the magnitude of maximum concentration of aerosols over poles and decreases with increase in the magnitude of tropical maximum. **(c, d)** Polar maximum causes enhanced precipitation. **(e, f)** Polar maximum causes enhanced precipitation minus evaporation. Results shown are averages of the last 30 yr of 60 yr simulations.

25409

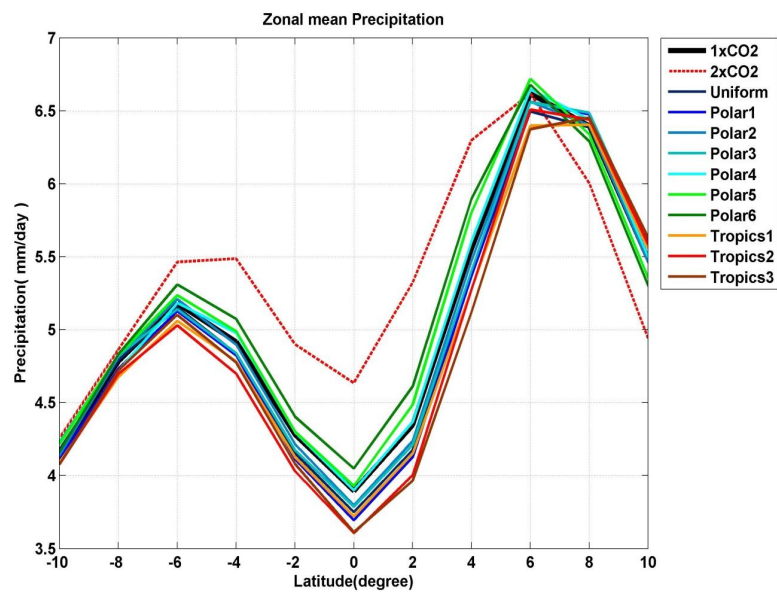


**Fig. 6.** Zonal mean precipitation over the globe. The position of intertropical convergence zone (ITCZ) remains the same in all the geoengineering cases. The zonal mean precipitation decreases monotonically over the equator as the global mean radiative forcing increases. Results shown are averages of the last 30 yr of 60 yr simulations.

25410

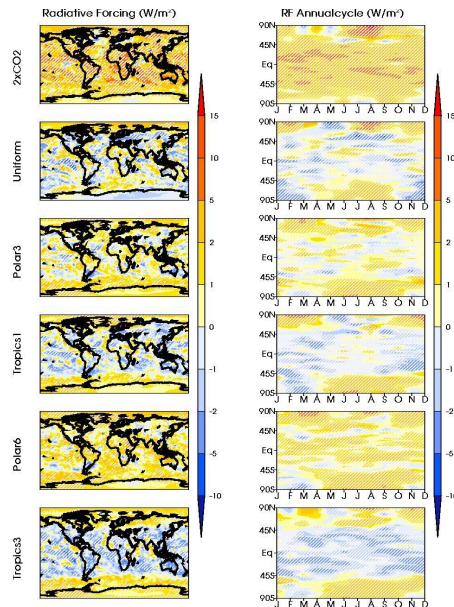


**Fig. 7.** Spatial pattern of radiative forcing (left panels) and the seasonal cycle of radiative forcing (right panels) in the  $2 \times \text{CO}_2$ , uniform, and some Polar and Tropics geoengineering scenarios. In the Uniform and Tropical cases, there is a residual positive forcing in the high latitudes and negative forcing in the low latitudes indicating an inexact compensation. The residual seasonal cycle is clearly visible in the polar regions in the Uniform case while in the Polar3 and Tropics1 cases the residual seasonal cycle has a much smaller strength. Hatching indicates the region where the changes are significant at 1% level. Significance level was estimated by Student  $t$  test. Results shown are averages of the last 20 yr of 30 yr simulations with fixed sea surface temperature and sea ice fraction.

25411

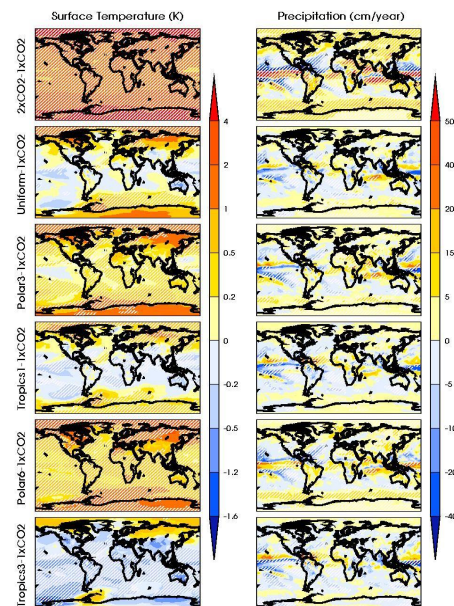


**Fig. 8.** Changes in annual-mean surface temperature (left panels) and precipitation (right panels) in the  $2 \times \text{CO}_2$ , uniform, and some Polar and Tropics geoengineering scenarios relative to the control ( $1 \times \text{CO}_2$ ). Hatching indicates the region where the changes are significant at 1% level. Significance level was estimated using Student  $t$  test. Both surface temperature and precipitation changes are large and significant everywhere in the  $2 \times \text{CO}_2$  and extreme scenarios (Polar6 and Tropics3). Although significant over large regions, both temperature and precipitation changes are small in the Uniform case. Polar3 scenario mitigates global mean precipitation but not global mean temperature while Tropics1 scenario mitigates global mean temperature but with reduced precipitation. Results shown are averages of the last 30 yr of 60 yr simulations.

25412

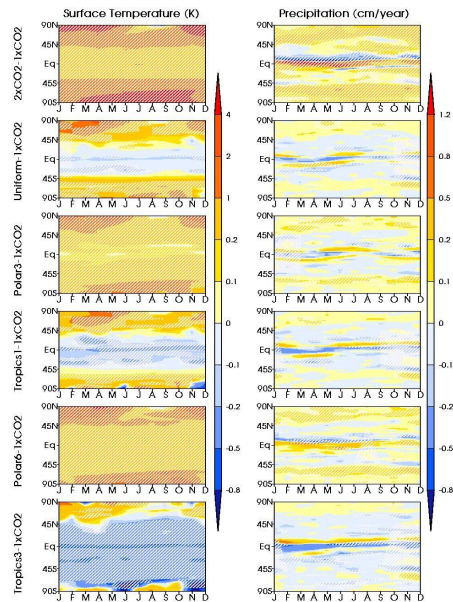


**Fig. 9.** Seasonal cycle of the changes in the zonally averaged surface temperature (left panels) and precipitation (right panels) in the  $2 \times \text{CO}_2$ , uniform and some Polar and Tropics geoengineering scenarios relative to the control ( $1 \times \text{CO}_2$ ). Seasonal variations in temperature response mostly occur in the high latitudes with larger warming in the winter and weaker warming in the summer. Hatching indicates the region where the changes are significant at 1% level. Significance level was estimated by Student  $t$  test. In case of surface temperature, the change in seasonal cycle is significant for both the Polar cases. Results shown are averages of the last 30 yr of 60 yr simulations.

25413

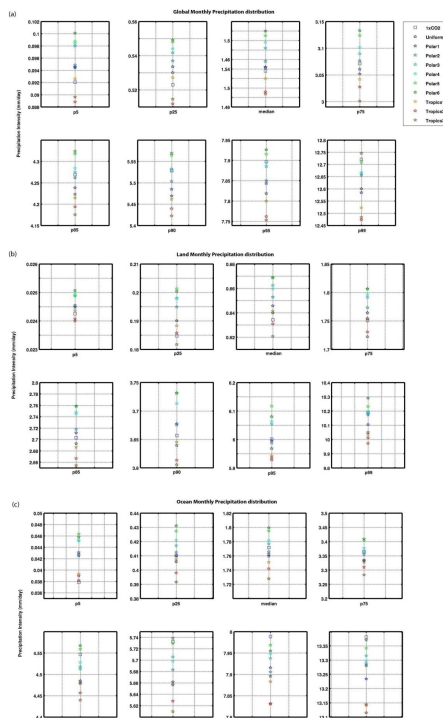


**Fig. 10.** Percentile values (p5, p25, median, p75, p85, p90, p95 and p99) of precipitation intensity over (a) Globe, (b) Land, (c) Ocean. There is a monotonic increase in precipitation for all percentile values as the maximum concentration of aerosols over poles increases. Grid-level monthly mean precipitation are used to calculate the percentile values. The last 30 yr of 60 yr simulations are used for the statistics.

25414

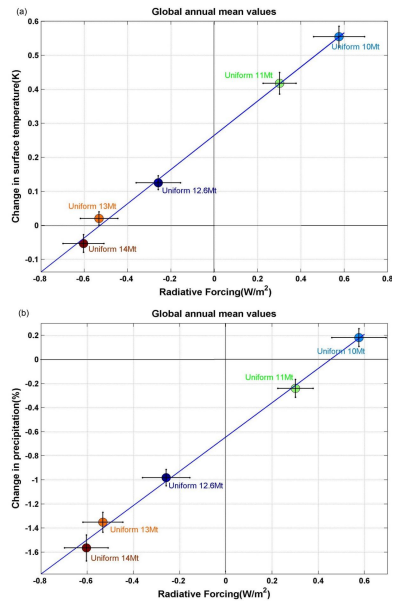


**Fig. 11. (a)** Radiative forcing (RF) vs. surface temperature change. **(b)** Radiative forcing vs. % precipitation change for uniform distribution scenarios with 10 Mt, 11 Mt, 12.6 Mt, 13 Mt and 14 Mt. More aerosol mass leads to negative residual radiative forcing and hence cooler and drier climate, and smaller aerosol mass leads to positive residual radiative forcing and hence warmer and wetter climate. In **(a)** and **(b)** the horizontal and vertical bars represent the standard error of the respective variables. Results shown are averages of the last 20 yr of 50 yr SOM simulations for temperature and precipitation while the last 20 yr of 40 yr fixed-SST simulations are used for radiative forcing calculations.

# **Sensitivity of Simulated Climate to latitudinal distribution of solar insolation reduction in **Solar Radiation Management****

Angshuman Modak\* and Govindasamy Bala

Divecha Centre for Climate Change & Centre for Atmospheric and Oceanic Sciences

Indian Institute of Science

Bangalore – 560 012, India

\*Corresponding author

Email: [amatcaos@caos.iisc.ernet.in](mailto:amatcaos@caos.iisc.ernet.in)



1 **Abstract**

2

3 Solar radiation management (SRM) geoengineering has been proposed as a potential  
4 option to counteract climate change. We perform a set of idealized geoengineering simulations  
5 using NCAR CAM3.1 to understand the global hydrological implications of varying the  
6 latitudinal distribution of solar insolation reduction in SRM methods. To reduce the solar  
7 insolation we have prescribed sulfate aerosols in the stratosphere. The radiative forcing in the  
8 geoengineering simulations is the net forcing from a doubling of CO<sub>2</sub> and the prescribed  
9 stratospheric aerosols. We find that for a fixed total mass of sulfate aerosols (12.6 Mt of SO<sub>4</sub>),  
10 relative to a uniform distribution which nearly offsets changes in global mean temperature from a  
11 doubling of CO<sub>2</sub>, global mean radiative forcing is larger when aerosol concentration is maximum  
12 at the poles leading to a warmer global mean climate and consequently an intensified  
13 hydrological cycle. Opposite changes are simulated when aerosol concentration is maximized in  
14 the tropics. We obtain a range of 1K in global mean temperature and 3% in precipitation changes  
15 by varying the distribution pattern in our simulations: this range is about 50 % of the climate  
16 change from a doubling of CO<sub>2</sub>. Hence, our study demonstrates that a range of global mean  
17 climate states, determined by the global mean radiative forcing, are possible for a fixed total  
18 amount of aerosols but with differing latitudinal distribution. However, it is important to note that  
19 this is an idealized study and thus not all important realistic climate processes are modeled.

20

21 (Key words: Climate Change, Geoengineering, Solar Radiation Management, Hydrological  
22 Cycle, Sulfate aerosols, Climate Model)

23

## 24 1. Introduction

25  
26 Atmospheric concentrations of the greenhouse gases (GHGs) such as carbon dioxide  
27 (CO<sub>2</sub>), methane (CH<sub>4</sub>) and nitrous oxide (N<sub>2</sub>O) have been increasing since pre-industrial periods  
28 primarily because of fossil fuel use and land-use change (IPCC, 2007). Their increase has the  
29 potential to cause long term climate change by altering the planetary radiation budget. To  
30 moderate future climate change and its impacts, several geoengineering proposals have been  
31 made recently. By definition, geoengineering is an intentional large-scale manipulation of the  
32 environment, particularly intended to counteract the undesired consequences of anthropogenic  
33 climate change (Keith, 2000).

34 Proposed geoengineering methods are classified into two main groups: Solar Radiation  
35 Management (SRM) methods and Carbon dioxide Removal (CDR) methods (Shepherd et al.,  
36 2009). In the first approach, the amount of solar absorption by the planet is reduced by  
37 artificially enhancing the planetary albedo so that the reduced insolation compensates the  
38 radiative forcing due to rising GHGs. Some proposed methods are injecting sulfate aerosols in  
39 the stratosphere (Budkyo, 1982; Crutzen, 2006; Wigley, 2006) and placing space based sun  
40 shields in between the Sun and the Earth (Early, 1989). CDR methods propose to accelerate the  
41 removal of CO<sub>2</sub> from the atmosphere and thus they deal with the root cause of global warming  
42 (Shepherd et al., 2009).

43 Past climate modeling studies have modeled the effects of space-based SRM methods by  
44 reducing the solar constant (Govindasamy and Caldeira, 2000; Matthews and Caldeira, 2007;  
45 Caldeira and Wood, 2008; Lunt et al., 2008) or modeled the effects of stratospheric aerosol  
46 methods (Robock et al., 2008; Rasch et al., 2008a; Rasch et al., 2008b; Heckendorn et al., 2009;  
47 Jones et al., 2010). It has been shown (e.g., Bala et al., 2008) that SRM geoengineering would  
48 lead to a weakening of the global water cycle when the global mean temperature change is offset  
49 exactly. A recent study (Tilmes et al., 2013) using 12 models from Geoengineering Model  
50 Intercomparison Project (GeoMIP) confirms this weakening of hydrological cycle under multi-  
51 model framework. Further, it has been shown (Robock et al., 2008; Ricke et al., 2010; Tilmes et  
52 al., 2013) that the level of compensation will vary with residual changes larger in some regions  
53 than others. Therefore, some recent studies (Ban-Weiss and Caldeira, 2010; MacMartin et al.,  
54 2012) determine an optimal reduction in solar radiation in both space and time so the

55 geoengineered world is more similar to the control climate while other studies (Irvine et al.,  
56 2010; Ricke et al., 2010) analyze the effect of different levels of uniform SRM forcing on  
57 regional climate response. Ban-Weiss and Caldeira (2010) vary both the amount and latitudinal  
58 distribution of aerosols to offset either the zonally averaged changes in surface temperature or the  
59 water budget. However, a simple and clear understanding of the effects of systematically varying  
60 the latitudinal distribution of aerosols and hence solar insolation reduction (e.g., more  
61 concentration in the tropics or high latitudes) on the hydrological cycle and surface temperature  
62 is lacking. In this study, we perform multiple idealized SRM geoengineering simulations with  
63 constant total amount of sulfate aerosols but with systematically varying latitudinal distribution.

64 We caution that our simulations are highly idealized and they are not meant to represent  
65 realistic latitudinal distribution of aerosols in geoengineering scenarios. Rather, they are designed  
66 to elucidate the fundamental properties of the climate system when the latitudinal distribution of  
67 aerosols and hence solar insolation reduction is systematically altered. We believe that our study  
68 should be considered as complementary to a previous work (Ban-Weiss and Caldeira, 2010),  
69 because not only we vary the latitudinal distribution of aerosols but we also provide a constraint  
70 by fixing the total amount of aerosols which facilitates a clear insight on the effects of varying  
71 the latitudinal distribution of aerosols.

72

## 73 **2. Model and Experiments**

74

75 We used the atmospheric general circulation model, CAM3.1 developed at the National  
76 Center for Atmospheric Research (NCAR) (Collins et al., 2004). It is coupled to the land model  
77 CLM3.0 and to a slab ocean model (SOM) with a thermodynamic sea ice model to represent the  
78 interactions with the ocean and sea ice components of the climate system. The model can be also  
79 configured with prescribed sea surface temperature and sea ice fraction. The horizontal resolution  
80 is  $2^\circ$  latitude and  $2.5^\circ$  longitude and the model has 26 vertical levels and the top of the model  
81 (TOM) is at 3hPa.

82 We performed two sets of simulations: 1) fixed-SST (sea surface temperature)  
83 simulations to estimate the radiative forcing which is measured as the net radiative flux change at  
84 the top of the atmosphere (Hansen et al., 1997). This method allows the rapid adjustment of the  
85 atmosphere and land components before radiative forcing is evaluated. The other set include the

86 SOM simulations to study the climate change. For both set of simulations, fixed-SST and SOM,  
87 we performed twelve cases: a control (1xCO<sub>2</sub>), doubled CO<sub>2</sub> climate (2xCO<sub>2</sub>) and ten  
88 geoengineering simulations each with differing latitudinal distribution of sulfate aerosol  
89 concentrations but with fixed total amount. The concentration of atmospheric CO<sub>2</sub> in 1xCO<sub>2</sub> is  
90 390ppm and is 780ppm in 2xCO<sub>2</sub> and geoengineering simulations. The concentrations of other  
91 greenhouse gases are kept constant in all simulations. The background sulfate aerosol amount in  
92 this version of the model is 1.38 Mt SO<sub>4</sub>. The fixed-SST simulations lasted for 30 years and the  
93 last 20 years are used to calculate the radiative forcing. The SOM simulations lasted for 60 years  
94 and the last 30 years are used for climate change analysis since all SOM simulations reach a  
95 near-equilibrium climate state in approximately 25 years.

96 As in Ban-Weiss and Caldeira (2010), the additional sulfate is prescribed in the  
97 geoengineering cases (Table 1, Figure 1a) and hence it is not transported around. However, in  
98 contrast to Ban-Weiss and Caldeira (2010), we introduce the constraint that the total amount of  
99 aerosol is constant (12.6 Mt SO<sub>4</sub>) while latitudinal distributions are varied. Since aerosols are  
100 prescribed at TOM, the effect is essentially equivalent to making latitudinal changes to the solar  
101 constant. Sulfate aerosol particle size is prescribed and is assumed to be log-normally distributed  
102 with dry median radius  $\approx 0.05\mu\text{m}$  and geometric standard deviation  $\approx 2.0$  (as used in a  
103 geoengineering scenario in a previous study (Rasch et al., 2008b)). The aerosol indirect effects  
104 are not modeled and aerosol loadings for other species like sea-salt, soil dust, black and organic  
105 carbon are unchanged in each of the simulations.

106 Besides a simulation with uniform aerosol concentration, our geoengineering simulations  
107 can be grouped into two categories: 1) Three “Tropics” simulations with maximum aerosol  
108 concentrations at the equator and 2) Six “Polar” cases with maximum concentrations at the poles.  
109 The latitudinal distribution of the stratospheric sulfate aerosol concentration are developed using  
110 the expression:

$$111 \quad Q(\varphi) = a + b\cos(\varphi)$$

112 where  $Q$  is the concentration of the additional mass of sulfate aerosols,  $a$  and  $b\cos(\varphi)$  are the  
113 uniform and non-uniform components of the distributions and  $\varphi$  represents the latitude. Both  $a$   
114 and  $b$  are varied to obtain various distributions of concentrations (Table 1, Figure 1a). However,  
115 when  $Q$  is integrated over the sphere, the result is 12.6Mt in all the cases. Our choice of 12.6 Mt  
116 for  $Q$  is dictated by the uniform distribution case which had near-zero global mean temperature

117 change relative to the control case. In each of the geoengineering simulations aerosol mass is  
118 added to the model background concentration at the TOM as was done in a recent study (Ban-  
119 Weiss and Caldeira, 2010). An experiment where the same total mass (12.6Mt) of aerosol is  
120 distributed uniformly over the globe between 61hPa to 9.8hPa (15 – 30km) with a maximum at  
121 30hPa (22km) showed that the radiative forcing is nearly the same as in our uniform distribution  
122 geoengineering case and hence the main conclusions reached in this study are unlikely to be  
123 altered.

124

### 125 3. Results

#### 126 3.1 Global mean Temperature and Precipitation Response

127

128 We find that the radiative forcing for doubling the atmospheric CO<sub>2</sub> (2xCO<sub>2</sub>) to be 3.5  
129 W/m<sup>2</sup> while the global mean surface temperature rise is about 2.1K and the precipitation increase  
130 is about 4.3% (i.e. ≈ 2%/K) in agreement with previous studies using the same model (Rasch et  
131 al., 2008b; Bala et al., 2009). The slopes in Figures 1c and 1d indicate a climate sensitivity of  
132 0.53K/Wm<sup>-2</sup> and precipitation sensitivity (% change in precipitation for unit change in radiative  
133 forcing) of 1.5%/Wm<sup>-2</sup> respectively, values that are similar to Bala et al. (2009).

134 The slight warming in the geoengineering case where forcing is close to zero (the case  
135 Polar 1 in Figure 1c) is because of the CO<sub>2</sub> physiological forcing (Betts et al., 2007; Cao et al.,  
136 2010) which is not counteracted by a decrease in solar flux. CO<sub>2</sub> physiological forcing refers to  
137 the direct physiological response of plants to elevated CO<sub>2</sub>: the plant stomata open less widely  
138 and thus decrease the canopy transpiration which in turn reduces evapotranspiration and causes  
139 surface warming. Therefore, in the zero radiative forcing case where CO<sub>2</sub> radiative forcing is  
140 countered by the reduction in solar radiation, the CO<sub>2</sub>-physiological forcing leads to a slight  
141 warming.

142 In agreement with past studies (e.g., Lunt et al., 2008; Bala et al., 2008; Tilmes et al.  
143 2013), we find that in the geoengineering scenario with uniform distribution of aerosol there is a  
144 decline in precipitation though there is a near cancellation of surface temperature change (Figure  
145 1b). This occurs because of differing fast response (changes that occur before global mean  
146 surface temperature) in precipitation for solar and CO<sub>2</sub>-forcing (Allen and Ingram, 2002; Bala et  
147 al., 2008; Bala et al., 2009; Andrews et al., 2009): longwave absorption by CO<sub>2</sub> in the

148 atmosphere can contribute to increased vertical stability and suppress precipitation but this fast  
149 response mechanism is nearly absent for solar forcing because the atmosphere is nearly  
150 transparent to solar radiation. However, since the slow response (changes that are associated with  
151 global mean surface temperature change) is same for CO<sub>2</sub> and solar forcings (Bala et al. 2010),  
152 the total changes in rainfall are larger to solar forcing than to equivalent CO<sub>2</sub> forcing. Because of  
153 this differing hydrological sensitivity to solar and CO<sub>2</sub> forcing, insolation reductions (in  
154 geoengineering scenarios) sufficient to offset the entirety of global-scale temperature increases  
155 would lead to a decrease in global mean precipitation. This suppression of precipitation is  
156 simulated in all geoengineering simulations (the regression line does not pass through the origin  
157 in Figure 1b).

158 Our geoengineering simulations with varying aerosol distributions indicate a linear  
159 relationship between the global mean surface temperature change and the precipitation change  
160 (Figure 1b). The regression lines do not pass through the origin which implies that none of the  
161 distribution can offset global mean temperature and precipitation simultaneously. Though the  
162 total amount of aerosols in each of the geoengineering simulation is fixed, we obtain a range of  
163 1K (residual cooling of 0.3 K for the Tropics3 case to residual warming of 0.7 K for the Polar6  
164 case) in global mean temperature and 3 % (residual drying of 2 % for Tropics3 case to residual  
165 increase of 1 % for the Polar6 case) in precipitation changes which are about 50 % or more of the  
166 changes that result from doubling of CO<sub>2</sub>. This indicates that a range of climate states are  
167 possible for a constant amount of aerosols.

168 As the polar maximum of the aerosol concentration increases the global mean  
169 temperature increases with concomitant increase in global mean precipitation as implied by the  
170 linear relationship in Figure 1b. One of the polar maximum SRM simulations (Polar3) almost  
171 offsets the changes in global mean precipitation but it has a residual warming of 0.4°C. Our  
172 results are broadly in agreement with other modeling studies: in an Arctic geoengineering study  
173 (Caldeira and Wood, 2008) with reduced solar constant only over arctic, residual global mean  
174 warming and enhancements of global precipitation are found.

175 In contrast, as magnitude of the tropical maximum concentration increases both global  
176 mean temperature and precipitation decreases. One of the Tropics cases (Tropics1) where the  
177 temperature change is nearly zero shows a reduction in the global mean precipitation. The  
178 reduction in precipitation in our “Tropics” simulations are consistent with observed decline in

179 precipitation over land, runoff and river discharge into the ocean following the tropical volcanic  
180 eruption Mount Pinatubo (15°N) in 1991 (Trenberth and Dai, 2007). Our “Tropics” simulations  
181 can be compared to Mount Pinatubo eruption because the distribution of aerosols in ‘Tropics’  
182 simulations have reasonable resemblance to the distribution of volcanic aerosols after few weeks  
183 of the eruption (the volcanic aerosols occupied a latitude band of 20° S to 30° N (McCormick et  
184 al., 1995)). Interestingly, we find that in none of the geoengineering scenarios considered in this  
185 study, changes in global mean surface temperature and precipitation can be offset simultaneously  
186 over either land or ocean. We also notice that the hydrological sensitivity (% change in  
187 precipitation per unit change in temperature) is almost same over both land and ocean (Figure  
188 1b). Here, we have defined the hydrological sensitivity over land (ocean) as the ratio of change in  
189 land (ocean) averaged precipitation to change in land (ocean) averaged surface temperature.

190 We find that the prescribed aerosols with different latitudinal distributions along with  
191 doubled CO<sub>2</sub> concentrations (geoengineering simulations) lead to different global mean forcings  
192 (Figure 1c and 1d). Since there are linear relationships between radiative forcing and the changes  
193 in global mean temperature (Figure 1c) and between temperature and precipitation changes  
194 (Figure 1b), we find a linear relationship between radiative forcing and precipitation changes  
195 (Figure 1d). The Polar geoengineering scenarios have positive residual radiative forcing while  
196 the Tropics scenarios have negative residual forcing because solar forcing is less effective over  
197 the poles relative to the tropics (Figure 1c). This is further confirmed in Figure 2 which shows  
198 that the Polar cases have smaller increase in planetary albedo compared to the Tropics cases. The  
199 radiative forcing associated with planetary albedo changes drive the temperature changes and  
200 thus the Polar cases have lower albedo changes relative to the uniform case and hence are  
201 warmer and wetter while opposite is true for Tropics cases.

202 The variation of global mean surface temperature and precipitation with global mean  
203 radiative forcing (Figure 1c and 1d) shows that as the maximum aerosol concentration over the  
204 poles increases (Polar1 to Polar6) the residual forcing increases and hence the global mean  
205 temperature and precipitation increase. Similarly, as the maximum aerosol concentration over  
206 the equator increases (Tropics1 to Tropics3), an opposite variation is noticed.

207 To further investigate the degree of departure of the different geoengineering simulations  
208 from the control, we calculate the root mean square difference between the *spatial patterns* in  
209 geoengineered climates and the control climate and normalize this root mean square difference

210 by the standard deviation of the control scenario (NRMSD). A value less than 1 for NRMSD  
211 would suggest that the geoengineered climate is indistinguishable from the control climate.  
212 Further, the geoengineering simulation with the smallest value for this quantity is the one that is  
213 closest to the control. In our study, we find that the NRMSD for temperature increases as the  
214 maximum concentration of aerosols at the poles increases and the NRMSD for precipitation  
215 increases as tropical maximum is increased (Figure 3). When all grids in the latitude-longitude  
216 domain are considered the NRMSD (Figure 3a) shows large variations: 0.40 to 1.4 for surface  
217 temperature and 0.25 to 0.40 for precipitation. In case of NRMSD for zonal means (Figure 3b),  
218 the spread is relatively less: 0.30 to 0.95 for surface temperature and 0.27 to 0.38 for  
219 precipitation. The uniform case has the least distance from the origin in Figure 3, suggesting that  
220 it has the least NRMSD if the objective is to minimize root mean square difference in both  
221 temperature and precipitation simultaneously.

222

### 223 **3.2 Precipitation and Temperature Response in Tropics and Poles**

224

225 The change in zonal-mean surface temperature between the geoengineering cases and the  
226 control case (1xCO<sub>2</sub>) show, similar to changes in global annual mean values, a monotonic  
227 increase at each latitude with increased polar weighting (Figure 4a). We notice a similar  
228 monotonic increase in zonal-mean land and zonal-mean ocean surface temperature (Figures 5a  
229 and 5b). Further, we find that almost all geoengineering simulation show residual high latitude  
230 warming. In the Tropics cases, we find smaller residual warming in the high latitudes and cooler  
231 tropics. Similar to temperature changes, the change in zonal-mean precipitation between the  
232 geoengineering cases and the control case show a monotonic increase at each latitude with  
233 increased polar weighting (Figures 4b, 5c and 5d). We find large changes in precipitation in the  
234 tropics which is likely to be seen as shifts in the intertropical convergence zone (ITCZ) but closer  
235 examination (Figure 6) shows that the position of ITCZ remains the same in all the cases and the  
236 monotonic increase in precipitation with poleward weighting is clearly seen. The changes in  
237 zonal mean precipitation minus evaporation (water budget) are similar to changes in zonal mean  
238 precipitation (Figures 4c, 5e and 5f).

239 Figure 7 shows the spatial pattern of radiative forcing in selected simulations: 2xCO<sub>2</sub>,  
240 Uniform, Polar3, Tropics1, Polar6 and Tropics3 cases. We notice that the radiative forcing in the



241 2xCO<sub>2</sub> case is significant over the whole globe but not significant in most regions in the  
242 geoengineering cases. The radiative forcing is positive in most locations in Polar cases. In the  
243 Tropics cases, the forcing is negative in the tropical regions and positive in polar regions.

244 In the 2xCO<sub>2</sub> case, both temperature and precipitation changes are large and significant  
245 over the whole globe (Figure 8). The temperature increase over poles is much larger than in the  
246 tropics, in agreement with previous studies (Caldeira and Wood, 2008; Lunt et al., 2008;  
247 Matthews and Caldeira, 2007; Robock et al., 2008; Rasch et al., 2008b). The uniform  
248 geoengineering case (Uniform) shows mitigation in the temperature with reduced precipitation  
249 relative to 1xCO<sub>2</sub>. This is because of the different nature of the CO<sub>2</sub> forcing and solar forcing:  
250 solar forcing is larger in the tropics and smaller in the poles whereas the CO<sub>2</sub> forcing is uniform  
251 over the whole globe. In Polar3 case, the change in precipitation is largely offset but there is  
252 significant warming over large regions. However, temperature is largely offset in Tropics1 but  
253 there is decrease in precipitation relative to the uniform distribution case. The last four panels of  
254 Figure 8 shows the extreme cases; the case with largest polar weighting (Polar6) significantly  
255 warms the planet while the case with largest tropical weighting (Tropics3) overcools the planet  
256 with large reduction in precipitation.

257

#### 258 **4. Discussion and Conclusions**

259

260 In this study, for a fixed total amount of sulfate aerosols which when distributed  
261 uniformly nearly offsets the global mean temperature change from a doubling of CO<sub>2</sub>, there is a  
262 residual cooling when the aerosol concentration is maximized near the tropical regions and  
263 warming when concentration is maximized near the polar regions (Figure 1c). Consequent  
264 changes in global mean precipitation are simulated as dictated by the hydrological sensitivity of  
265 the model (Figure 1b). Our result that the global mean precipitation is reduced when aerosol  
266 concentration is maximized at the equator is in agreement with a recent study that shows a drastic  
267 reduction in tropical rainfall when aerosol concentration is maximum in the tropics (Ferraro et al.  
268 2014). We also observe a similar monotonic increase in precipitation intensity as the maximum  
269 aerosol concentration over the poles increases (Figure 9, 10 and 11). The increases are of the  
270 order of 10% for low intensity (5<sup>th</sup> percentile) and 2-3% for large intensity (99<sup>th</sup> percentile)  
271 between the extreme cases (Tropics3 and Polar6). In order to confirm that global mean radiative

272 forcing is sufficient to infer the global mean climate change we performed four additional  
273 geoengineering simulations with total amount of aerosols varied (10Mt, 11Mt, 13Mt, and 14Mt)  
274 for the uniform distribution case. We find that the global mean temperature and precipitation  
275 changes follow the changes in global mean forcing (Figure 12) for this set of simulations too.

276 In agreement with earlier studies (e.g., Bala et al., 2008), we find that both temperature  
277 and precipitation changes cannot be offset simultaneously. In agreement with this, not only in a  
278 simulation with uniform distribution but in all the geoengineering simulation with different  
279 latitudinal distribution (that is, even with non-uniform distribution of solar insolation reduction),  
280 we find that it is not possible to offset both temperature and precipitation changes  
281 simultaneously. The latitudinal distribution which offsets the warming leads to a drier climate  
282 while the distribution which offsets the precipitation results in a relatively warmer world (note  
283 that Bala et al. (2008) used a uniform solar insolation reduction). For a fixed total amount of  
284 aerosols but with different latitudinal distribution it is possible to achieve a range of global mean  
285 radiative forcing and thus a range of climate states.

286 Our findings should be viewed in the light of the limitations and uncertainties involved in  
287 this study. Our simulations are highly idealized as we have prescribed sulfate aerosol (to reduce  
288 the solar insolation) instead of injecting and transporting them. We have prescribed a fixed  
289 particle size distribution but particle size distribution would evolve with time and is shown to be  
290 important in precisely estimating the effects on different climate variables (Rasch et al., 2008b).  
291 Some modeling studies (Robock et al., 2008) have injected aerosol precursors into the  
292 stratosphere with fixed particle size distribution while other studies (Heckendorn et al., 2009;  
293 Pierce et al., 2010; Niemeier et al., 2010; Hommel and Graf, 2011; English et al., 2012) have  
294 demonstrated the importance of including the microphysics of particle growth. Further, we have  
295 focused our investigation primarily on global mean climate while several other studies (e.g.,  
296 Robock et al., 2008; Irvine et al., 2010; Ricke et al., 2010) focused on regional disparities.

297 In this study, we have not considered the consequences of detailed stratospheric dynamics  
298 and sulfate aerosol chemistry on the ozone layer (Tilmes et al., 2009). Our model lacks a  
299 dynamic ocean and sea ice components, and thus the effects of deep ocean circulation are not  
300 modeled here. Further, in this model an interactive land carbon cycle is not included and hence  
301 the impact of changes in the diffuse fraction of surface solar radiation due to stratospheric

302 aerosols could not be investigated. We intend to use a later version of the model that includes  
303 carbon cycle to investigate the impacts of altered diffuse radiation in a future study. However, we  
304 believe our results on temperature and precipitation is so fundamental that they would be  
305 unchanged when additional components and feedbacks are included.

306 In summary, for a fixed total mass of aerosols, we find that the global mean climate is  
307 warmer and wetter when aerosol concentration is maximum over the poles relative to the uniform  
308 distribution case (which offsets global mean temperature change) because the global mean  
309 residual radiative forcing is positive in these cases when compared to the uniform case. The  
310 opposite is true when aerosol concentration is maximum in the tropics. Further, our study clearly  
311 indicates that knowledge of global mean radiative forcing, not the details of latitudinal  
312 distribution of aerosols, is sufficient to infer the global mean climate change.

313

314 *Acknowledgements.* Financial support for A. Modak was provided by the Divecha Centre for  
315 Climate Change, Indian Institute of Science. We thank the Supercomputer Education and  
316 Research Centre, Indian Institute of Science for providing the computational resources.

317

## 318 **References**

- 319 1. Allen, M.R. and Ingram, W. J.: Constraints on future changes in climate and the hydrologic  
320 cycle, *Nature*, 419, 224-232, doi:10.1038/nature01092, 2002.
- 321 2. Andrews, T., Forster, P. M., and Gregory, J. M.: A surface energy perspective on climate  
322 change, *J. Climate.*, 22, 2557-2570, doi: 10.1175/2008JCLI2759.1, 2009.
- 323 3. Bala, G., Caldeira K., and Nemani, R.: Fast versus slow response in climate change:  
324 implications for the global hydrological cycle, *Clim. Dynam.* 35, 423-434, doi:  
325 10.1007/s00382-009-0583-y, 2009.
- 326 4. Bala, G., Duffy P. B., and Taylor, K. E.: Impact of geoengineering schemes on the global  
327 hydrological cycle, *P. Natl. Acad. Sci. USA*, 105, 7664-7669, doi:10.1073/pnas.0711648105,  
328 2008.
- 329 5. Ban-Weiss, G. A. and Calderia, K.: Geoengineering as an Optimization Problem, *Environ.*  
330 *Res. Lett.*, 5, 034009, doi:10.1088/1748-9326/5/3/034009, 2010.
- 331 6. Betts, R. A., Boucher, O., Matthew, C., Cox, P. M., Falloon, P. D., Gedney, N., Hemming, D.  
332 L., Huntingford, C., Jones, C. D., Sexton, D. M. H., and Webb, M. J.: Projected increase in  
333 continental runoff due to plant responses to increasing carbon dioxide, *Nature*, 448, 1037–  
334 1041, doi:10.1038/nature06045, 2007.
- 335 7. Budkyo, M.I.: *The Earth's Climate Past and Future*, Academic, 1982.
- 336 8. Caldeira, K. and Wood, L.: Global and Arctic climate engineering: Numerical model studies,  
337 *Philos. T. Roy. Soc. A*, 366, 4039-4056, doi: 10.1098/rsta.2008.0132, 2008.

- 338 9. Cao, L., Bala, G., and Caldeira, K.: Climate response to changes in atmospheric carbon  
339 dioxide and solar irradiance on the time scale of days to weeks, *Environ. Res. Lett.*,7,  
340 034015, doi:10.1088/1748-9326/7/3/034015, 2012.
- 341 10. Cao, L., Bala, G., Caldeira, K., Nemani, R., and Ban-Weiss, G. A.: Importance of carbon  
342 dioxide physiological forcing to future climate change, *P. Natl. Acad. Sci.*  
343 USA,doi:10.1073/pnas.0913000107, 2010.
- 344 11. Collins, W. D., Rasch, P. J., Boville, B. A., Hack, J. J., McCaa, J. R., Williamson, D. L.,  
345 Kiehl, J. T., Briegleb, B., Bitz, C., Lin, S-J., Zhang, M., and Dai, Y.: Description of the  
346 NCAR community atmosphere model (CAM 3.0) NCAR Tech. Rep. NCAR/TN-464+STR  
347 National Center for Atmospheric Research Boulder CO 226pp, 2004.
- 348 12. Crutzen, P.J.: Albedo enhancement by stratospheric sulfur injections: A contribution to  
349 resolve a policy dilemma?, *Climatic Change*, 77, 211-220, doi: 10.1007/s10584-006-9101-y,  
350 2006.
- 351 13. Early, J.T.: Space-based solar shield to offset greenhouse effect, *Journal of the British*  
352 *Interplanetary Society*, 42, 567-569, 1989.
- 353 14. English, J. M., Toon, O. B., and Mills, M. J.: Microphysical simulations of sulfur burdens  
354 from stratospheric sulfur geoengineering, *Atmos. Chem. Phys.*,12, 4775-4793,  
355 doi:10.5194/acp-12-4775-2012, 2012.
- 356 15. Ferraro, A. J., Highwood, E. J., and Charlton-Perez, A. J.: Weakened tropical circulation and  
357 reduced precipitation in response to geoengineering. *Environ. Res. Lett.*, 9, 014001 doi:  
358 10.1088/1748-9326/9/1/014001, 2014.
- 359 16. Govindasamy, B. and Caldeira, K.: Geoengineering Earth's radiation balance to mitigate  
360 CO<sub>2</sub>-induced climate change, *Geophys. Res. Lett.*, 27, 2141–2144, 2000.
- 361 17. Hansen, J., Sato, M., and Ruedy, R.: Radiative forcing and climate response *J. Geophys. Res.*,  
362 102(D6) 6831–6864, 1997.
- 363 18. Heckendorn, P., Weisenstein, D., Fueglistaler, S., Luo, B. P., Rozanov, E., Schraner, M.,  
364 Thomason, L. W., and Peter, T.: The impact of geoengineering aerosols on stratospheric  
365 temperature and ozone, *Environ. Res. Lett.*, 4, 045108, doi: 10.1088/1748-9326/4/4/045108,  
366 2009.
- 367 19. Hommel, R. and Graf, H. F.: Modelling the size distribution of geoengineered stratospheric  
368 aerosols, *Atmos. Sci. Lett.*, 12, 168-175, doi: 10.1002/asl.285, 2011.
- 369 20. Irvine, P. J., Ridgwell, A., and Lunt, D. J.: Assessing the regional disparities in  
370 geoengineering impacts, *Geophys. Res. Lett.*, 37, L18702, doi: 10.1029/2010GL044447,  
371 2010.
- 372 21. IPCC 2007 Climate Change 2007: The Physical Science Basis Contribution of Working  
373 Group 1 to the Fourth Assessment Report of the Intergovernmental Panel on Climate Change  
374 ed S Solomon, D Qin, M Manning, Z Chen, M Marquis, K B Averyt, M Tignor and H L  
375 Miller (Cambridge & New York: Cambridge University Press) 996 pp.
- 376 22. Jones, A., Haywood, J., Boucher, O., Kravitz, B., and Robock, A.: Geoengineering by  
377 stratospheric SO<sub>2</sub> injection: Results from the Met Office HadGEM2 climate model and  
378 comparison with the Goddard Institute for Space Studies ModelE, *Atmos. Chem. Phys.*  
379 *Discuss.*, 10, 7421-7434, doi: 10.5194/acpd-10-7421-2010, 2010.
- 380 23. Keith, D. W.: Geoengineering the climate: history and prospect, *Annu. Rev. Energ. Env.*, 25,  
381 245–284, 2000.

- 382 24. Lunt, D. J., Ridgwell, A., Valdes, P. J., and Seale, A.: ‘Sunshade world’: a fully coupled  
383 GCM evaluation of the climatic impacts of geoengineering, *Geophys. Res. Lett.*, 35, L12710,  
384 doi: 10.1029/2008GL033674, 2008.
- 385 25. Matthews, H. D. and Caldeira, K.: Transient climate-carbon simulations of planetary  
386 geoengineering, *P. Natl Acad. Sci. USA*, 104, 9949–9954, doi: 10.1073/pnas.0700419104,  
387 2007.
- 388 26. MacMartin, D. G., Keith, D.W., Kravitz, B., and Caldeira, K.: Management of trade-offs in  
389 geoengineering through optimal choice of non-uniform radiative forcing, *Nature Climate*  
390 *Change*, doi: 10.1038/nclimate1722, 2012.
- 391 27. McCormick, M. P., Thomason, L. W., and Treppe, C. R.: Atmospheric effects of the Mt.  
392 Pinatubo eruption, *Nature*, 373, 399–404, 1995.
- 393 28. Niemeier, U., Schmidt, H., and Timmreck, C.: The dependency of geoengineered sulfate  
394 aerosol on the emission strategy, *Atmos. Sci. Lett.*, 12, 189–194, doi: 10.1002/asl.304, 2010.
- 395 29. Pierce, J. R., Weisenstein, D. K., Heckendorn, P., Peter, T., and Keith, D.W.: Efficient  
396 formation of stratospheric aerosol for climate engineering by emission of condensable vapor  
397 from aircraft, *Geophys. Res. Lett.*, 37, L18805, doi: 10.1029/2010GL043975, 2010.
- 398 30. Rasch, P. J., Tilmes, S., Turco, R. P., Robock, A., Oman, L., Chen, C.C., Stenchikov, G.L.,  
399 and Garcia, R. R.: An overview of geoengineering of climate using stratospheric  
400 sulphate aerosols, *Philos. T. Roy. Soc. A*, 366, 4007–4037, doi: 10.1098/rsta.2008.0131,  
401 2008a.
- 402 31. Rasch, P. J., Crutzen, P. J., and Coleman, D. B.: Exploring the geoengineering of climate  
403 using stratospheric sulfate aerosols: The role of particle size, *Geophys. Res. Lett.*, 35,  
404 L02809, doi: 10.1029/2007GL032179, 2008b.
- 405 32. Robock, A., Oman, L., and Stenchikov, G. L.: Regional climate responses to geoengineering  
406 with tropical and Arctic SO<sub>2</sub> injections, *J. Geophys. Res.*, 113, D16101, doi:  
407 10.1029/2008JD010050, 2008.
- 408 33. Rieke, K. L., Morgan, M. G., and Allen, M. R.: Regional climate response to solar-radiation  
409 management, *Nature Geosci.*, 3, 537 – 541, 2010.
- 410 34. Shepherd, J., Caldeira, K., Haigh, J., Keith, D., Launder, B., Mace, G., MacKerron, G., Pyle,  
411 J., Rayner, S., Redgwell, C., and Watson, A.: *Geoengineering the climate: science,*  
412 *governance and uncertainty*, The Royal Academy, 2009.
- 413 35. Tilmes, S., Garcia, R. R., Kinnison, D. E., Gettelman, A., and Rasch, P. J.: Impact of  
414 geoengineered aerosols on the troposphere and stratosphere, *J. Geophys. Res.*, 114, D12305,  
415 doi: 10.1029/2008JD011420, 2009.
- 416 36. Tilmes et al.: The hydrological impact of geoengineering in the Geoengineering Model  
417 Intercomparison Project (GeoMIP). *J. Geophys. Res. Atmos.*, 118, 11,036–11,058, doi:  
418 10.1002/jgrd.50868, 2013.
- 419 37. Trenberth, K.E. and Dai, A.: Effects of Mount Pinatubo volcanic eruption on the hydrological  
420 cycle as an analog of geoengineering, *Geophys. Res. Lett.*, 34, L15702, doi:  
421 10.1029/2007GL030524, 2007.
- 422 38. Wigley, T. M. L.: A combined mitigation/geoengineering approach to climate stabilization,  
423 *Science*, 314, 452–454, doi: 10.1126/science.1131728, 2006.

424 **Figure Captions**

425  
426 **Figure 1:** (a) Latitudinal profiles of sulfate aerosol concentration in the SRM geoengineering  
427 experiments. Polar1-6 have maximum concentration over the poles and Tropics1-3 have  
428 maximum at the equator. (b) Surface temperature change (K) vs precipitation change (%) relative  
429 to the 1xCO<sub>2</sub> case from slab ocean simulations ( global mean values - squares, land mean values  
430 - stars, ocean mean values - triangles) . There is warming in all Polar cases relative to the uniform  
431 case and a concomitant increase in precipitation. Opposite is the case for Tropics cases. None of  
432 the regression lines pass through origin; temperature and precipitation cannot be offset  
433 simultaneously. In the case of land and ocean,  $\Delta T_S$  and  $\Delta P$  represent the averages over the  
434 respective domain. (c) Radiative forcing (RF) vs surface temperature change. Polar cases have  
435 larger forcing relative to the uniform case and hence are warmer while opposite is true for  
436 Tropics cases. (d) Radiative forcing vs % precipitation change. Precipitation increases with  
437 residual RF (i.e. with increase in polar weighting) while decreases with increase in tropical  
438 weighting. In (b), (c) and (d) the horizontal and vertical bars represent the standard error of the  
439 respective variables which are calculated from the last 30 years of 60-year SOM simulations  
440 while in case of radiative forcing it is calculated from the last 20 years of 30-year fixed-SST  
441 simulations.

442  
443 **Figure 2:** Change in planetary albedo in fixed-SST vs surface temperature change in slab ocean  
444 geoengineering simulations. The radiative forcing associated with albedo changes drive the  
445 temperature changes. Polar cases have lower albedo changes relative to the uniform case and  
446 hence are warmer and wetter while opposite is true for Tropics cases. The horizontal and vertical  
447 bars represent the standard error of the respective variables; temperature standard errors are  
448 calculated from the last 30 years of 60-year SOM simulations while albedo standard errors are  
449 calculated from the last 20 years of 30-year fixed-SST simulations.

450  
451  
452 **Figure 3:** Normalized root mean square difference (NRMSD) of surface temperature and  
453 precipitation between geoengineering and control simulation normalized by respective standard  
454 deviations computed for the global domain (top panel) and for the zonal averages (bottom panel).

455 The annual means of the last 30 years of the 60-year control simulation are used to estimate the  
456 standard deviation. Simulation nearest to x-axis represents the best precipitation mitigating  
457 scenario while the one closest to y-axis represents the best surface temperature mitigating  
458 scenario. Scenarios with maximum aerosol concentrations at the poles have larger NRMSD in  
459 temperature and conversely simulations with maximum at the equator have larger NRMSD in  
460 precipitation.

461

462 **Figure 4:** Zonal means of change in surface temperature ( $\Delta TS$ ), precipitation ( $\Delta P$ ) and  
463 precipitation minus evaporation ( $\Delta PmE$ ). (a) Zonal mean  $\Delta TS$  increases monotonically with  
464 increase in maximum concentrations over the poles and decreases with increase in tropical  
465 maxima. (b) Zonal mean  $\Delta P$ : polar maximum causes enhanced precipitation. (c) Zonal mean  
466  $\Delta PmE$ ; polar maximum causes enhanced precipitation minus evaporation. Results shown are  
467 averages of the last 30 years of 60-year simulations.

468

469 **Figure 5:** Changes in zonal mean surface temperature ( $\Delta TS$ ), precipitation ( $\Delta P$ ) and  
470 precipitation minus evaporation ( $\Delta PmE$ ) over ocean (left panels) and land (right panels). (a) and  
471 (b): Zonal mean  $\Delta TS$  increases monotonically with increase in the magnitude of maximum  
472 concentration of aerosols over poles and decreases with increase in the magnitude of tropical  
473 maximum. (c) and (d): polar maximum causes enhanced precipitation. (e) and (f): polar  
474 maximum causes enhanced precipitation minus evaporation. Results shown are averages of the  
475 last 30 years of 60-year simulations.

476

477 **Figure 6:** Zonal mean precipitation over the globe. The position of intertropical convergence  
478 zone (ITCZ) remains the same in all the geoengineering cases. The zonal mean precipitation  
479 decreases monotonically over the equator as the global mean radiative forcing increases. Results  
480 shown are averages of the last 30 years of 60-year simulations.

481

482 **Figure 7:** Spatial pattern of radiative forcing in the  $2xCO_2$ , uniform, and some Polar and Tropics  
483 geoengineering scenarios. In the Uniform and Tropical cases, there is a residual positive forcing  
484 in the high latitudes and negative forcing in the low latitudes indicating an inexact compensation.  
485 Hatching indicates the region where the changes are significant at 1% level. Significance level

486 was estimated by Student's t test. Results shown are averages of the last 20 years of 30-year  
487 simulations with fixed sea surface temperature and sea ice fraction.

488  
489 **Figure 8:** Changes in annual-mean surface temperature (left panels) and precipitation (right  
490 panels) in the 2xCO<sub>2</sub>, uniform, and some Polar and Tropics geoengineering scenarios relative to  
491 the control (1xCO<sub>2</sub>). Hatching indicates the region where the changes are significant at 1% level.  
492 Significance level was estimated using Student's t-test. Both surface temperature and  
493 precipitation changes are large and significant everywhere in the 2xCO<sub>2</sub> and extreme scenarios  
494 (Polar6 and Tropics3). Although significant over large regions, both temperature and  
495 precipitation changes are small in the Uniform case. Polar3 scenario offsets global mean  
496 precipitation but not global mean temperature while Tropics1 scenario offsets global mean  
497 temperature but with reduced precipitation. Results shown are averages of the last 30 years of 60-  
498 year simulations.

499  
500 **Figure 9:** Percentile values (p5, p25, median, p75, p85, p90, p95 and p99) of precipitation  
501 intensity over Globe. There is a monotonic increase in precipitation for all percentile values as  
502 the maximum concentration of aerosols over poles increases. Grid-level monthly mean  
503 precipitation are used to calculate the percentile values. The last 30 years of 60-year simulations  
504 are used for the statistics.

505  
506 **Figure 10:** Percentile values (p5, p25, median, p75, p85, p90, p95 and p99) of precipitation  
507 intensity over Land. There is a monotonic increase in precipitation for all percentile values as the  
508 maximum concentration of aerosols over poles increases. Grid-level monthly mean precipitation  
509 over all land points are used to calculate the percentile values. The last 30 years of 60-year  
510 simulations are used for the statistics.

511  
512 **Figure 11:** Percentile values (p5, p25, median, p75, p85, p90, p95 and p99) of precipitation  
513 intensity over Ocean. There is a monotonic increase in precipitation for all percentile values as  
514 the maximum concentration of aerosols over poles increases. Grid-level monthly mean  
515 precipitation over all ocean points are used to calculate the percentile values. The last 30 years of  
516 60-year simulations are used for the statistics.



517 **Figure 12:** (a) Radiative forcing (RF) vs surface temperature change. (b) Radiative forcing vs %  
518 precipitation change for uniform distribution scenarios with 10Mt, 11Mt, 12.6Mt, 13Mt and  
519 14Mt. More aerosol mass leads to negative residual radiative forcing and hence cooler and drier  
520 climate, and smaller aerosol mass leads to positive residual radiative forcing and hence warmer  
521 and wetter climate. In (a) and (b) the horizontal and vertical bars represent the standard error of  
522 the respective variables. Results shown are averages of the last 20 years of 50-year SOM  
523 simulations for temperature and precipitation while the last 20 years of 40-year fixed-SST  
524 simulations are used for radiative forcing calculations.

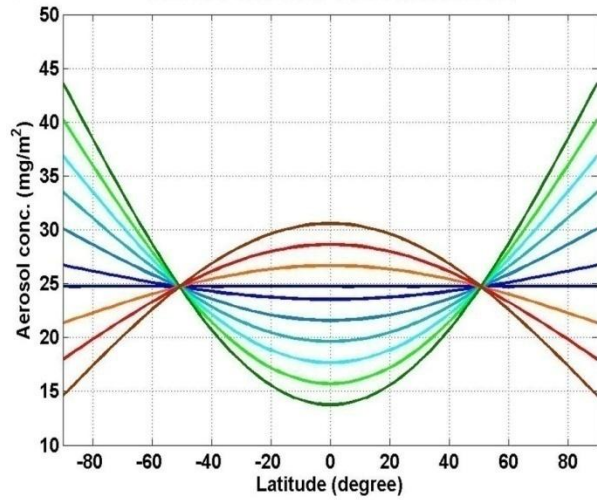
525 **Table 1:** Description of different geoengineering experiments. Total additional mass is 12.6 Mt  
 526 SO<sub>4</sub> in all the geoengineering simulations but the distribution varies.

<b>Name of the Experiments</b>	<b>a (mg/m<sup>2</sup>)</b>	<b>b (mg/m<sup>2</sup>)</b>	<b>Total Mass from uniform component (Mt)</b>	<b>Total Mass from non-uniform component (Mt)</b>	<b>Total Mass (Mt)</b>
<b>Uniform</b>	24.70	-	12.60	-	12.60
<b>Polar1</b>	23.52	3.19	12.00	0.60	12.60
<b>Polar2</b>	21.56	8.55	11.00	1.60	12.60
<b>Polar3</b>	19.60	13.89	10.00	2.60	12.60
<b>Polar4</b>	17.64	19.22	9.00	3.60	12.60
<b>Polar5</b>	15.68	24.56	8.00	4.60	12.60
<b>Polar6</b>	13.72	29.90	7.00	5.60	12.60
<b>Tropics1</b>	26.66	-5.34	13.60	-1.00	12.60
<b>Tropics2</b>	28.62	-10.67	14.60	-2.00	12.60
<b>Tropics3</b>	30.58	-16.02	15.60	-3.00	12.60

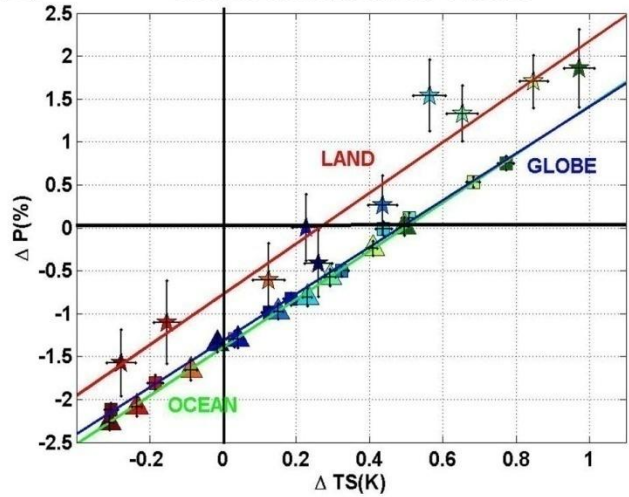
527  
 528

Figure 1

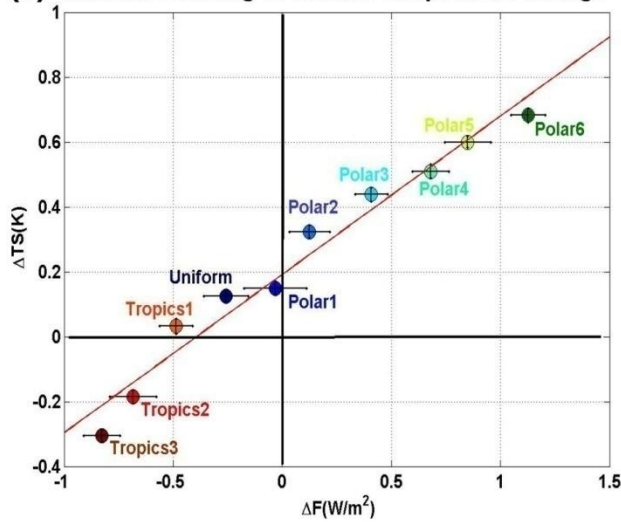
(a) Sulfate aerosol concentrations



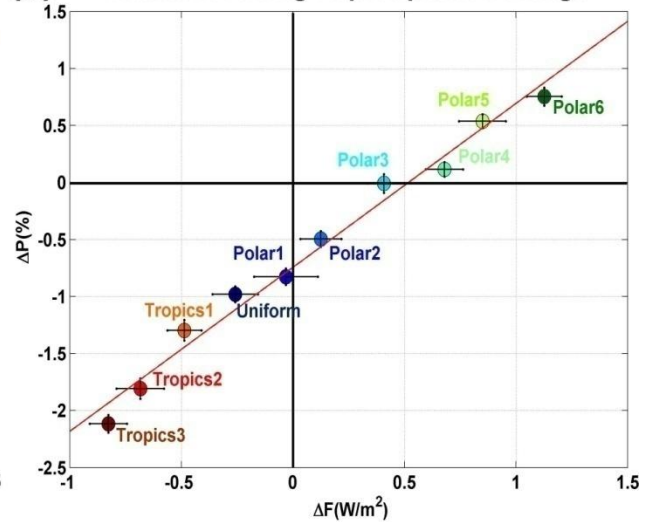
(b) Global annual mean values



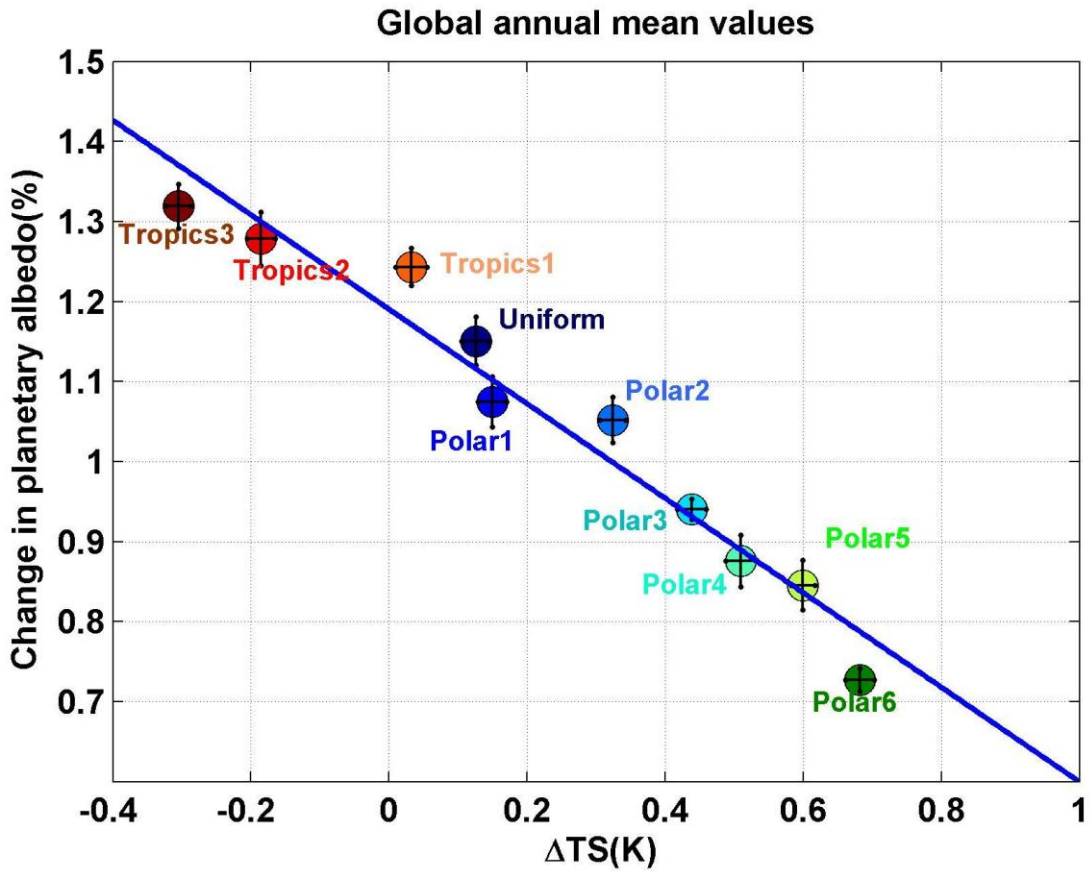
(c) Radiative forcing vs surface temperature change



(d) Radiative forcing vs precipitation change

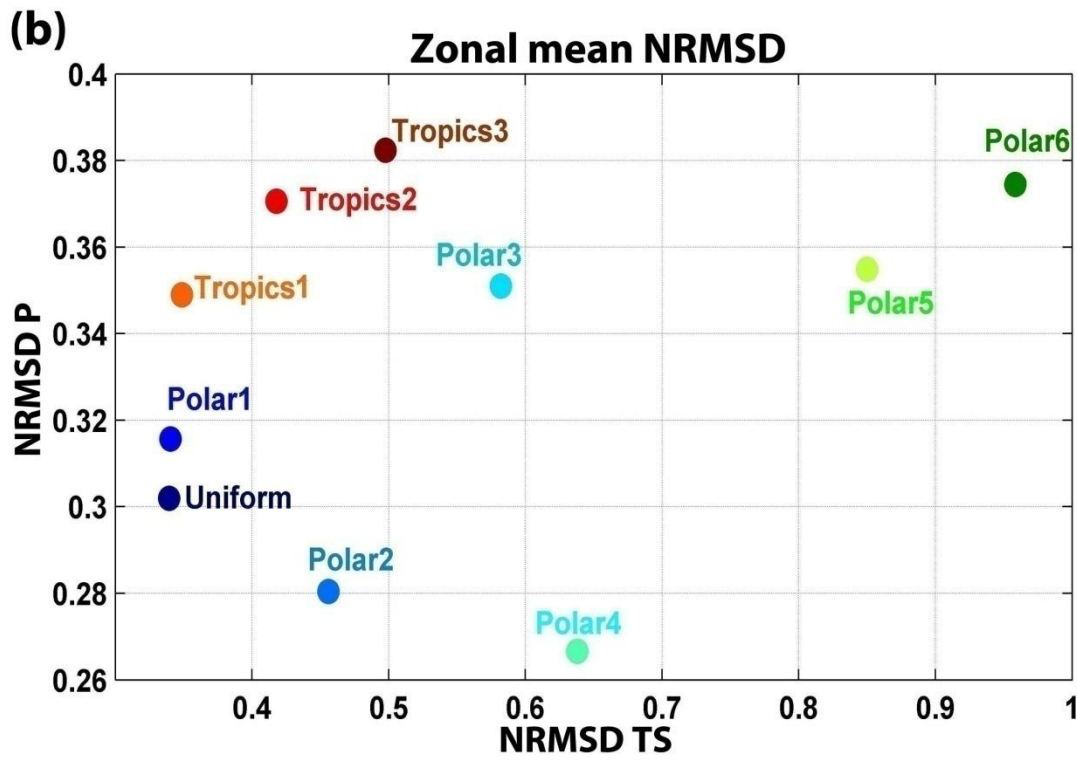
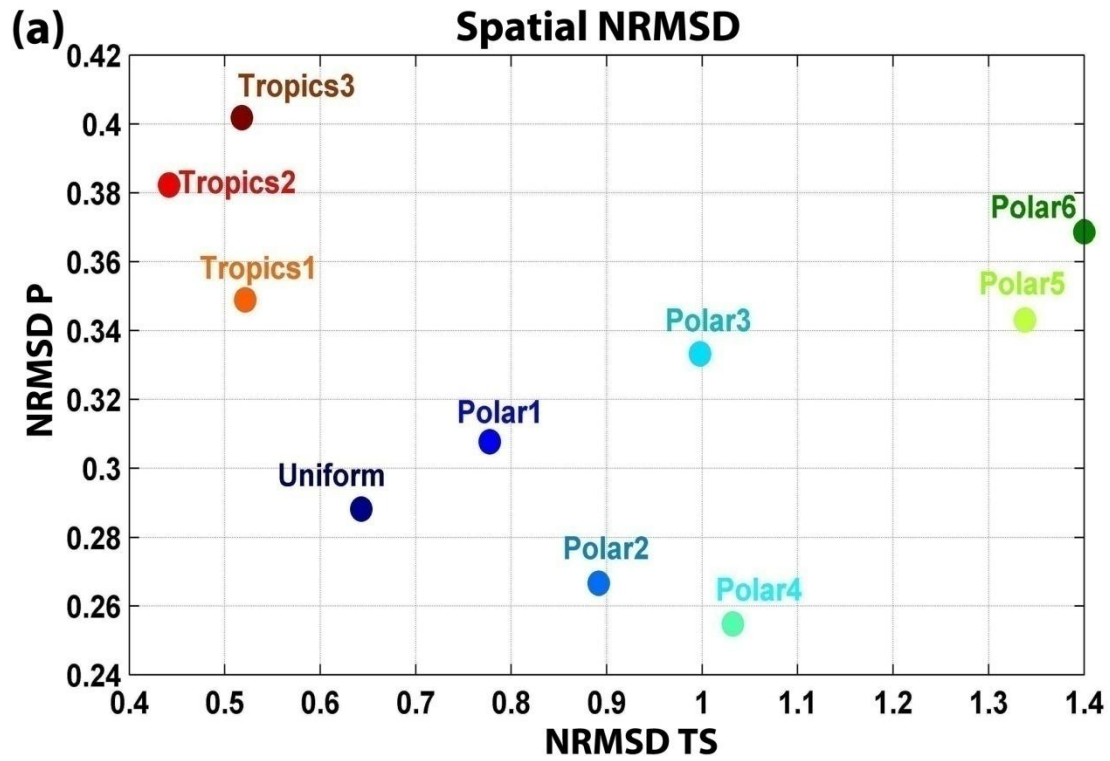


531 Figure 2



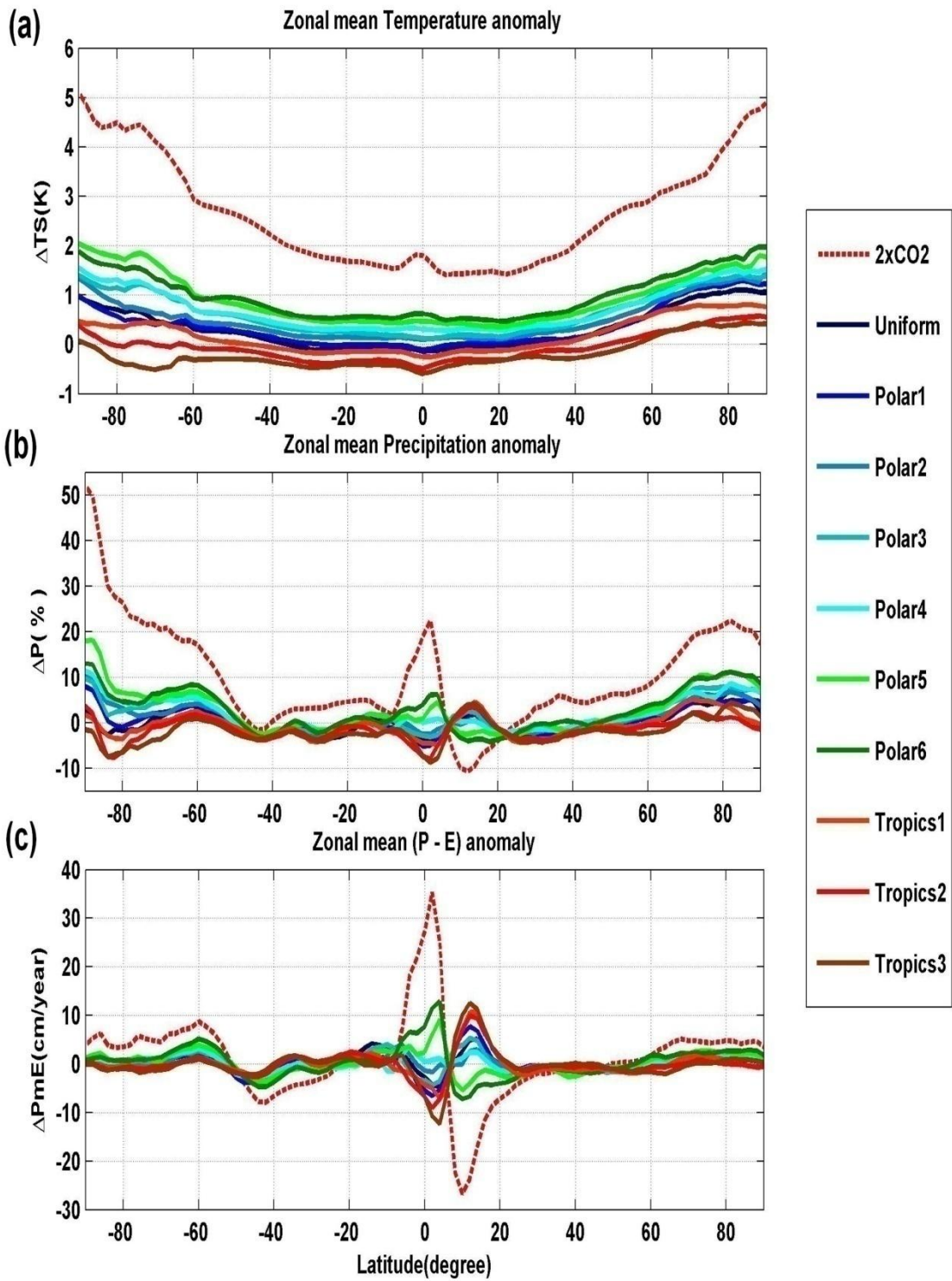
532  
533

534 Figure 3



535

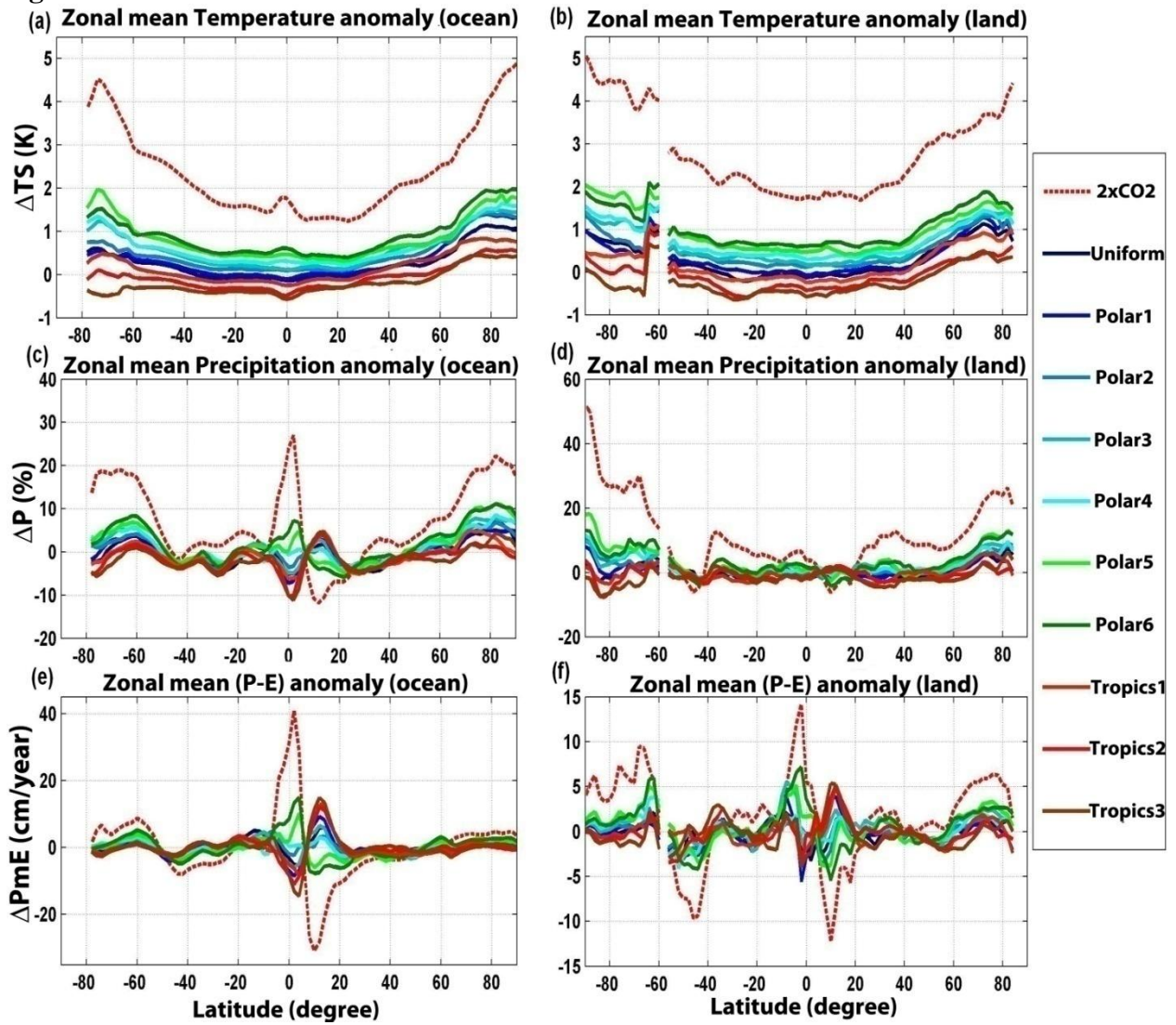
536 **Figure 4**



537  
538

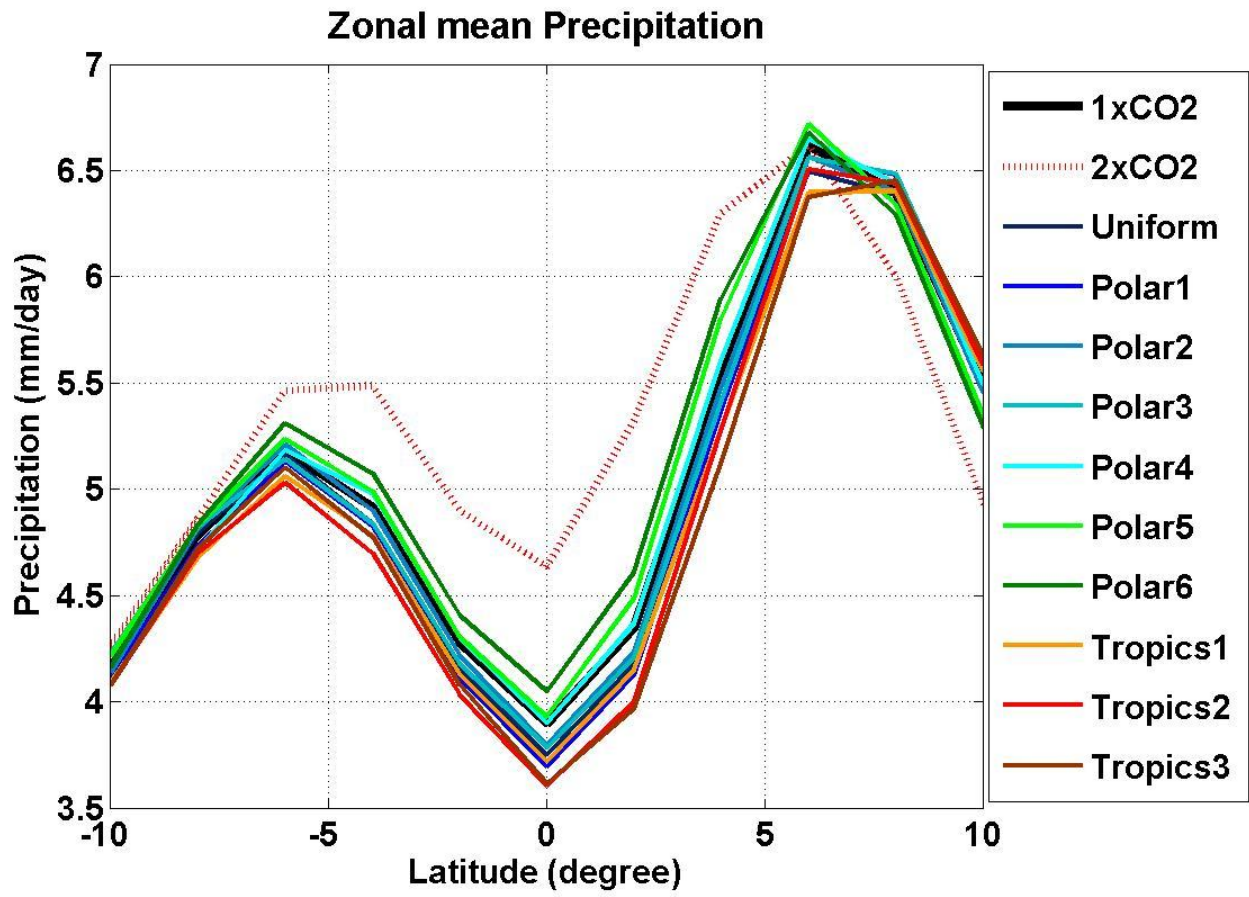
539

Figure 5



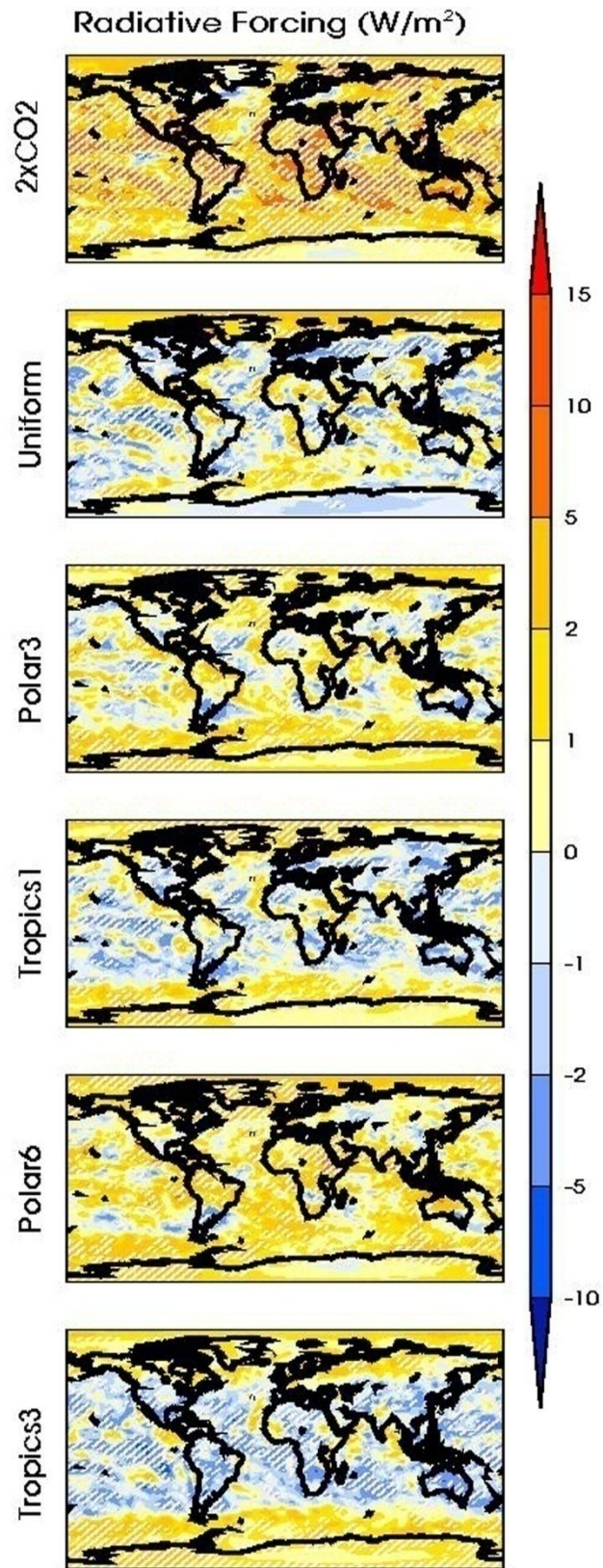
540  
541

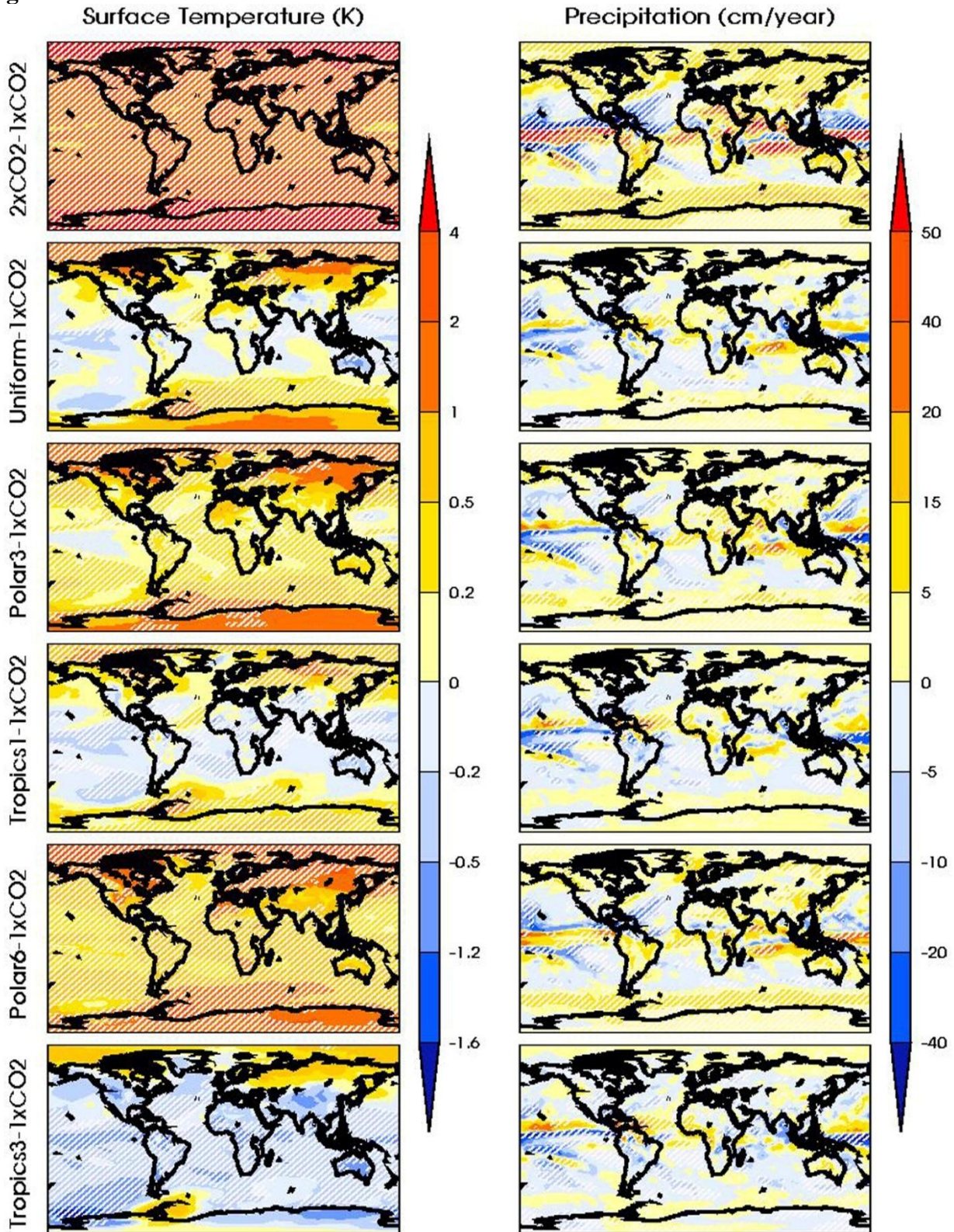
542 Figure 6



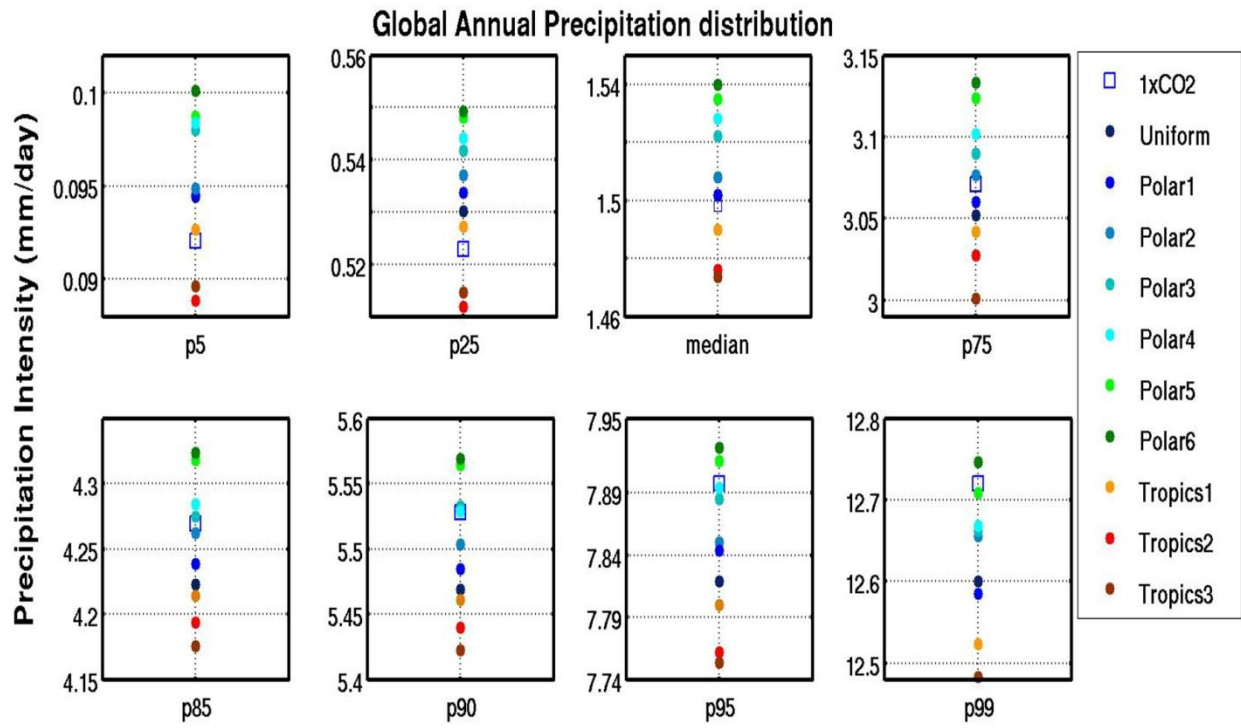
543  
544





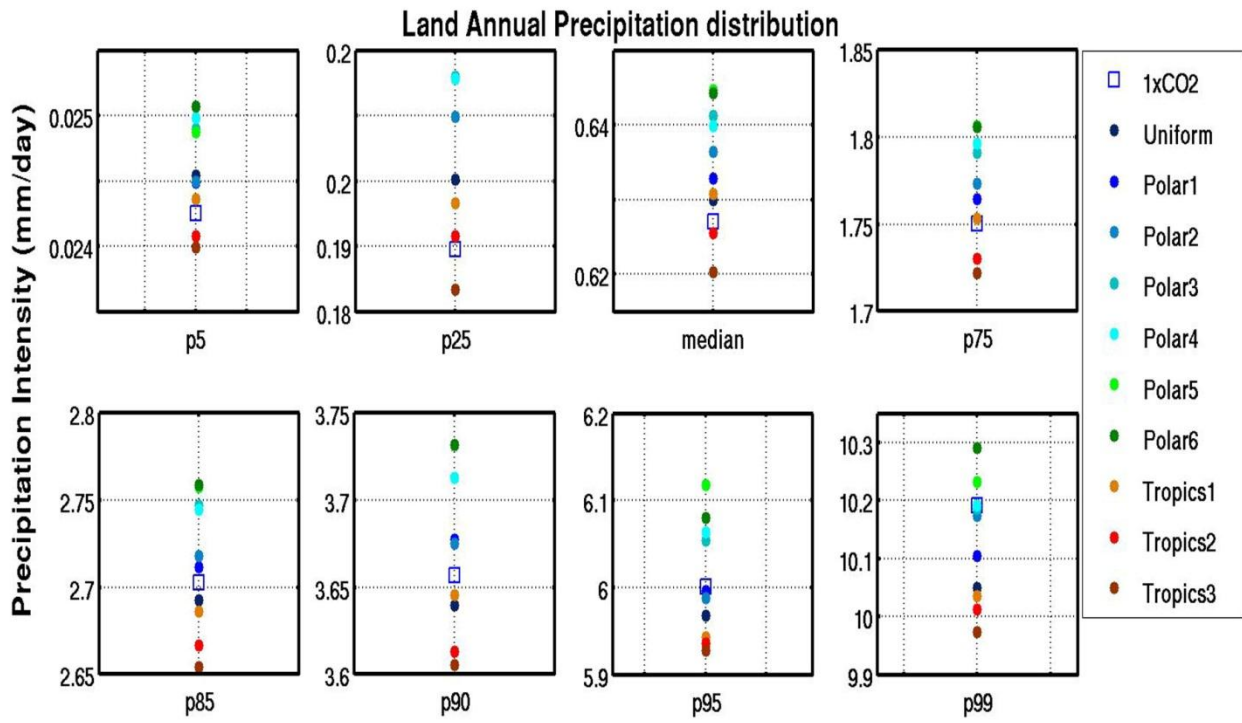


550 **Figure 9**



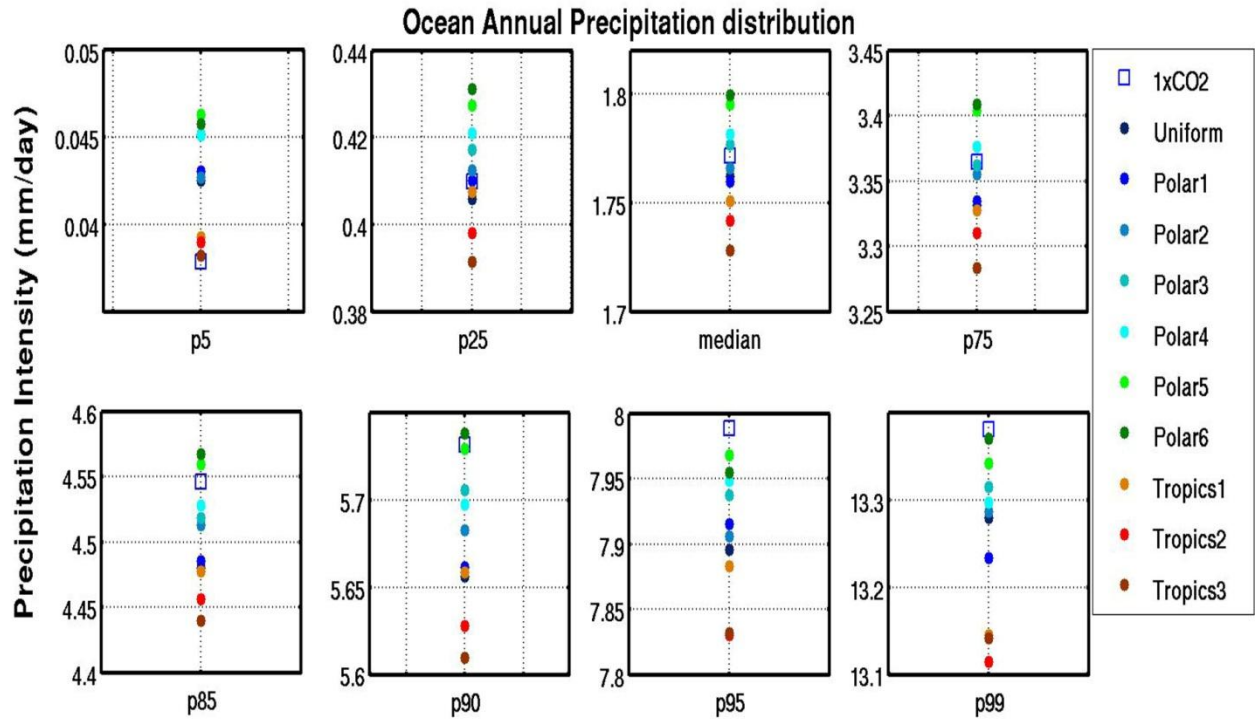
551  
552

553 **Figure 10**



554  
555

556 **Figure 11**



557  
558

